The conundrum of hot mitochondria

David Macherel, Francis Haraux, Hervé Guillou, Olivier Bourgeois

BBA Bioenergetics 2020

The conundrum of hot mitochondria

David Macherel[a*], Francis Haraux[b], Hervé Guillou[c], Olivier Bourgeois[c]

[a] IRHS-UMR1345, Université d'Angers, INRAE, Institut Agro, SFR 4207 QuaSaV, 49071, Beaucouzé, France

[b] Institute for Integrative Biology of the Cell, Université Paris-Saclay, 91191 Gif-sur-Yvette, France

[c] Université Grenoble Alpes et Institut Neel, Université Grenoble Alpes et CNRS, 25 rue des Martyrs, 38042 Grenoble, France

* Corresponding author: david.macherel@univ-angers.fr.

Abstract

Mitochondrion is often referred as the cellular powerhouse because the organelle oxidises organic acids and NADH derived from nutriments, converting around 40% of the Gibbs free energy change of these reactions into ATP, which is the major energy currency for cell metabolism. Mitochondria are thus microscopic furnaces that inevitably release heat as a by-product of these reactions, which contributes to body warming, especially in endotherms like birds and mammals, which evolved exquisite mechanisms of control to regulate their temperature. For a decade now, the idea emerged that mitochondria could be warmer than their immediate surroundings, i.e. the cytosol, because of their intense metabolic activity as energy transducers. It was even suggested that our own mitochondria could operate in normal conditions at a temperature close to 50°C. That an increase in the temperature of a micrometre furnace could be explained by the laws of thermal physics was hotly debated.

Here, we aimed, as biologists and physicists, to exhaustively review the reports that led to the concept of a hot mitochondrion, which is essentially based on the development and use of a variety of molecular thermosensors which intrinsic fluorescence is modified by temperature. We also discuss the physical concepts of heat diffusion, including mechanisms occurring at the nanoscale range like phonons scattering. Although we could not reconcile the hypothesis of hot mitochondria and physical point of view, we nevertheless put forward some possible directions to explore further this intriguing conundrum.

Keywords

Mitochondria, oxidative phosphorylation, heating, Fourier's law, thermosensor

Abbreviations

ANT, adenine nucleotide translocase; AOX, alternative oxidase; BAT, brown adipose tissue; BMR, basal metabolic rate; DPPC, di-palmitoyl-phosphatidylcholine; ETC, electron transfer chain; ER, endoplasmic reticulum; FLIM, fluorescence life time imaging; GFP, green fluorescent protein; MTY, Mito Thermo Yellow probe; OXPHOS, oxidative phosphorylation; ROS, reactive oxygen species; TCA, tricarboxylic acid cycle; UCP, uncoupling protein

1. Introduction

Endotherms have the capacity to maintain a relatively high and constant body temperature under a wide range of ambient conditions using thermal energy released by metabolic reactions. The emergence of endothermy and sophisticated mechanisms of body thermal regulation led to the evolutionary success of birds and mammals, whose warm bodies allowed high physiological activity and locomotor ability even under cold conditions [1]. Endotherms require a high basal metabolic rate to sustain body heat production and, accordingly, their food requirements are on average 30 times greater than for equivalent-sized ectotherms [2]. Most body heat in endotherms originates from the operation of oxidative phosphorylation in mitochondria, whose efficiency can be adapted to modulate heat production under specific conditions [1,3]. Core body temperature in endotherms is normally very stable, apart from diel variations and where animals are able to hibernate. Where body temperature falls outside these norms, it is often related to disease, as has been recognised since antiquity in the case of fever, for example, and from the late 19th century thermometric measurements became an essential part of clinical examination [4]. While some parts of the body in endotherms (periphery, surface, appendages…) are clearly cooler than the core body temperature, there are also variations in the temperature of different organs depending on their activity and insulation. There is some heterogeneity of human core body temperature, with a narrow range of around 0.5°C between measuring sites, while inter-individual variation can reach 1.5-2.4°C under basal conditions [5]. It was thus surprising when a manuscript entitled "*Mitochondria are physiologically maintained at close to 50°C*" appeared in 2017 on BioRxiv (DOI: 10.1101/133223), before its final publication in PLoS Biology [6], accompanied by a relevant primer [7]. In this paper, the temperature of mitochondria appeared to be 10°C higher than that of their fibroblast host cells grown at 37°C. Although this was not the first time that mammalian mitochondria had been suggested to be warmer than their surroundings (see [8,9]), such a discovery fostered attention and discussion, especially considering the thermal physics of the phenomenon (e.g. [10]). The concept of hot mitochondria behaving as cellular radiators is indeed fascinating, and we wish here to review the underlying principles, facts and perspectives. After presenting the principles of biological heat production and endothermy, we will review the published research about measurements of mitochondrial temperature, and extend the discussion about thermal physics, with its limits and possible openings with respect to the nanoscale of the mechanisms of mitochondrial heat generation. Finally, we will attempt to propose future directions that might challenge the hot hypothesis of warmer mitochondria.

2. Principles of biological heat production

Life, energy and heat are indissociably linked by the laws of thermodynamics because organisms are open systems which are highly organized, and thus require an input of high-grade energy to ensure

their maintenance, growth and reproduction. Feeding or photosynthesis furnishes chemical energy to fuel metabolism, which consists of a myriad of orchestrated chemical reactions that sustain the life processes of every organism, including various physiological functions. It is remarkable that metabolic rates, which are negatively correlated with mass, only display a 30-fold variation (from 0.3 to 9 W kg^{-1}) across organisms whose masses can vary over 20 orders of magnitude (from bacteria to elephants); this extraordinary convergence of metabolic rates demonstrates that energy fluxes are very similar in all forms or life [11]. The cellular energy supply is provided by catabolism, which consists of a controlled degradation of complex molecules like carbohydrates, lipids or proteins by a process during which the Gibbs free energy change of these reactions is used to drive the regeneration of ATP, the universal energy currency of cells. Most of the reactions involved in catabolism are exothermic, and thus release heat as a by-product. Indeed, as early as 1789 Lavoisier deduced from pioneering calorimetric experiments that "respiration is a combustion, admittedly very slow, but nevertheless completely analogous to that of charcoal" [12]. Oxidative phosphorylation (OXPHOS), which is the major provider of ATP in eukaryotic cells, has a thermodynamic efficiency close to 40% in animal cells, however it is calculated [13]. This implies that 60% of the energy input is released as low grade energy, i.e. heat. While it is unquestionable that the operation of OXPHOS potentially releases significant amounts of heat, one must remain aware that determining the actual OXPHOS efficiency remains very difficult, and the actual figure could be very variable depending on metabolic situations (Nicholls and Ferguson 2013).

Most organisms, like prokaryotes, fungi, protists, plants, invertebrates and cold-blooded animals are ectotherms, which means that, although they do generate metabolic heat, they are generally unable to maintain their temperature higher than that of the environment. This suggests that their metabolic heat production diffuses too fast to contribute to cell and tissue warming. In contrast, homeotherms like mammals and birds have evolved the capacity to maintain a high and stable temperature (37-39°C depending on species), which provides a major advantage by allowing them to remain active in a wide range of environmental temperatures. Homeotherms have evolved exquisite neuroregulatory sensing and signalling networks to precisely adjust core body temperature, which is achieved both by regulation of endothermy and of thermal distribution and exchange by the blood circuitry [14]. Since thermal distribution is shared by most other animal ectotherms, metabolic activity should be the major component of homeothermy; this is metabolically very expensive since the organisms need to produce large amounts of heat to maintain their temperature, and thus to consume large amounts of food. This is well illustrated by the fact that small mammals, which lose heat rapidly because of their large surface/volume ratio, have much faster metabolic and heart rates than bigger mammals, and under cold conditions they have to dedicate most of their energy expenditure to defending their body temperature [15,16].

More than 60 years ago, mitochondria were first coined the powerhouses of the cell [17], which illustrates the fact that these organelles are the centres of energy transduction in the eukaryotic cell, and as such provide a major contribution to body heat production. Indeed, in the so-called indirect calorimetry approach the oxygen consumption rate is used as a proxy to deduce the production of heat and external work of animals with a conversion factor of around 20 J/ml O_2 [11,18]. For homeotherms, the basal metabolic rate (BMR), which is recorded when resting and fasting in thermoneutral conditions, reflects the thermodynamic cost of maintenance while the daily energy expenditure (DEE) also takes into account the full energetic cost of life including all activities [19]. For ectotherms, the equivalent of BMR is standard metabolic rate (SMR), which is measured for fasting and resting animals at the environmental temperature. As thoroughly discussed in a seminal review [3], most metabolic heat production originates at the inner mitochondrial membrane where OXPHOS takes place (Figure 1A, B).

During OXPHOS (Figure 1C), NADH generated in the matrix by the pyruvate dehydrogenase complex and tricarboxylic acid (TCA) cycle enzymes is oxidized by the electron transfer chain (ETC) of the inner mitochondrial membrane. Complex I (NADH ubiquinone oxidoreductase) oxidizes NADH, and the electrons are then transferred to ubiquinone, complex III, cyt *c*, and finally cytochrome oxidase which reduces O_2 into H_2O. Complex II (succinate ubiquinone oxidoreductase; succinate dehydrogenase) directly oxidizes succinate to fumarate, the electrons being transferred to ubiquinone via a FAD prosthetic group. At the level of complex I, III and IV, the transfer of electrons is energetically and mechanistically coupled to the export of protons, which results in a stoichiometry of 10 $H^+/2\ e^-$ or 8 $H^+/2\ e^-$ depending on whether the ETC is fed with NADH or succinate. The resulting proton gradient (ΔP) with its chemical (ΔpH) and electrical components ($\Delta\Psi$) generates the protonmotive force (Pmf), which is able to power endergonic ATP synthesis [20]. This last step of OXPHOS is carried out by ATP synthase, which allows protons to flow back to the matrix space, harnessing their energy as a turbine to catalyse the phosphorylation of ADP. The detailed thermodynamic constraints and their impact on the activity and regulation of OXPHOS were thoroughly reviewed earlier [21]. OXPHOS could theoretically achieve a high energy efficiency, i.e. converting most of the energy of substrates into ATP, if the coupling between ETC, proton gradient and ATP synthesis was perfect. However, this is never the case because there is always a basal proton leakage across the mitochondrial inner membrane, which thus bypasses ATP synthase and dissipates the proton gradient without contributing to ATP synthesis [22]. Proton leakage is well illustrated by the fact that isolated mitochondria oxidize supplied substrates at a stable and significant rate (so-called state 4), even when ATP synthase is inhibited by oligomycin. The leakage is known to occur essentially through adenine nucleotide translocase (ANT) as an intrinsic and regulated function distinct from adenylate exchange [23]. The mechanism of proton leakage by ANT appears to be

negatively regulated by nucleotide exchange activity, which allows an increase in the energy efficiency of OXPHOS when ATP demand is high.

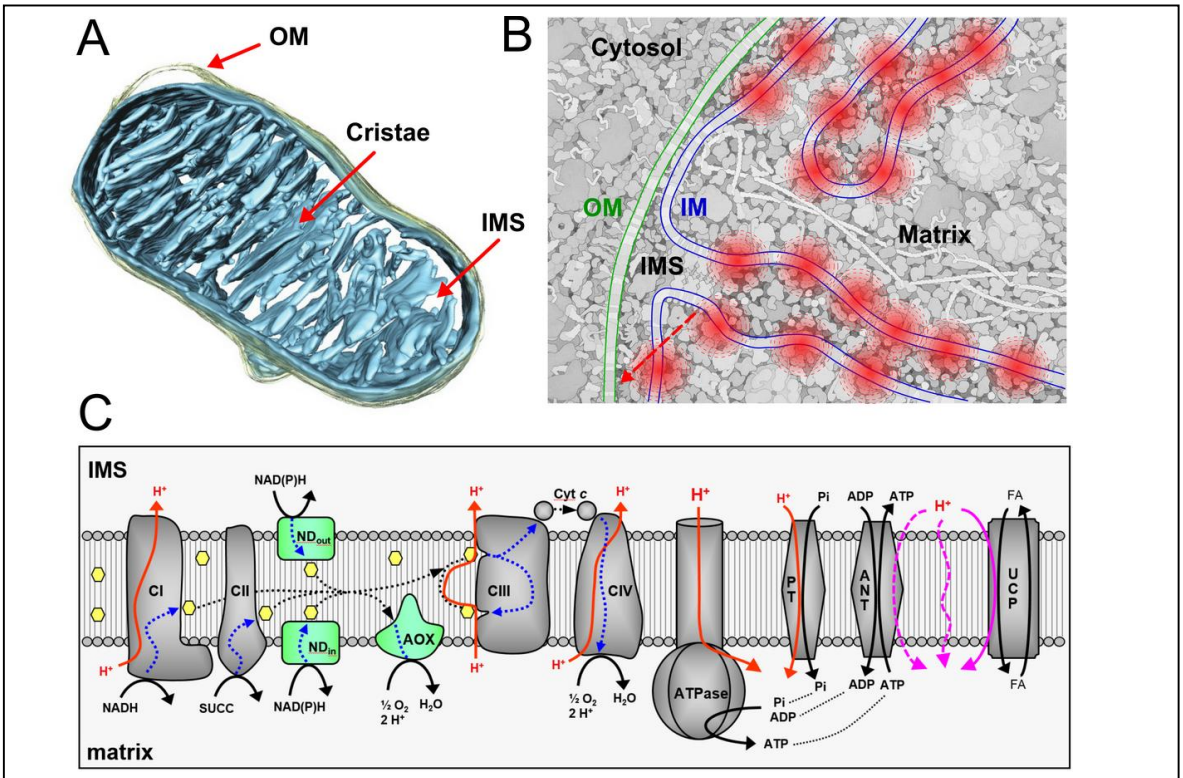

Figure 1. The mitochondrial scene. Panel A shows the 3D segmented volume of a heart mitochondrion from a 20 week-old mice that was obtained by electron cryo-tomography [98]. Outer membrane appears in yellowish gray and cristae in blue. Reproduced from Figure 2 in [98], published under the Creative Commons Attribution 4.0 International Public License (CC BY 4.0; https://creativecommons.org/licenses/by/4.0/). Panel B is a drawing of a section of a mitochondrion figuring macromolecular crowding according to [99]. The original colour drawing was converted to greyscale, and the delimitation of mitochondrial membranes (approximately 6 nm thickness) was indicated with green traits for outer membrane (OM) and blue traits for inner membrane (IM). The heat production at the level of the inner membrane is tentatively suggested by the concentric red zones. It must be stressed, however, that almost nothing is known about the actual sites of heat production at the molecular level. Panel C shows the mechanism of oxidative phosphorylation (OXPHOS), including components expected to play a role in mitochondrial heat generation. The alternative dehydrogenases (ND_{in} and ND_{out}) and the alternative oxidase (AOX) which are also present in mitochondria from plants, fungi and protists are shown in green. Ubiquinones (oxidised or reduced) are shown as yellow hexagons. Electron transfer within complexes is indicated by dotted blue arrows, active proton transfer by red arrows. Purple arrows refer to proton leakage, either passive (dash) or catalysed by uncoupling protein

Proton leakage is a futile cycle (proton pumping and leakage) that generally contribute to 15-50% of the respiratory rate in different mammalian tissues, and its contribution to the BMR can reach 20-25% [24]. Proton leakage uncouples ATP generation from substrate oxidation, which increases heat production by mitochondria. The energy of leaking protons cannot be converted into biochemical work (ATP synthesis), but rather sustain futile proton pumping (and electron transfer) by the ETC, resulting in an increase in random motion and molecular collisions, generating heat. Heat production reaches its maximum when mitochondria are fully uncoupled by chemicals or UCP activation because the rate of electron transfer and proton pumping gets out of control, and since no work can be done, all energy is released as heat. The persistence during evolution of a mechanism that reduces the energy efficiency of mitochondria suggests it must play a critical role, which is likely involved in limiting reactive oxygen species (ROS) production in mitochondria [24]. Inevitably, electron transfer leads to a side reaction that converts O_2 into the ROS superoxide, especially at the levels of complex I and III, a reaction that is amplified as ΔP increases, and that can lead to oxidative stress if ROS detoxication mechanisms are overwhelmed. By limiting ΔP when ATP demand is low, proton leakage avoids excessive ROS production, and possibly also avoids $\Delta\Psi$ becoming too high, since a typical potential of 200 mV across a 5 nm-thick membrane is equivalent to 40 kV/mm, a value in the range of the dielectric strength (i.e. the maximum field a material can withstand) of most common insulators. Proton leakage can also be induced by specialized mitochondrial uncoupling proteins (UCPs) that can dissipate the proton gradient by a mechanism based on free fatty acid cycling, and which is regulated by purine nucleotides [25]. UCP1, which is considered the archetypal UCP, is highly expressed in thermogenic tissues of mammals such as brown adipose tissue (BAT), where it can trigger heat production by uncoupling mitochondria. This non-shivering thermogenesis is activated in response to cold by neuronal circuits and noradrenaline, which activates lipolysis, and mitochondrial biogenesis [26]. BAT is generally found in small mammals like rodents and in newborns of larger mammals for which adaptive thermogenesis is crucial, but it is also present in human adults [27]. Other UCPs (UCP2, UCP3 in mammals) are expressed in mammalian tissues, and UCP orthologs were discovered in many taxonomic groups of endothermic and ectothermic animals, plants, and protists, but there is no clear evidence for a role of these proteins in thermogenesis [28]. Non-shivering thermogenesis also occurs in the skeletal muscles of animals by several mechanisms of energy dissipation like futile creatine cycling, sarcoplasmic Ca^{2+} ATPase and sodium-potassium pump, which also enhance mitochondrial activity and thus heat production [29,30]. This short overview of heat generation highlights the central role of mitochondria in endothermic animals as furnaces, in which basal heat production can be boosted by energy-dissipating mechanisms such as uncoupling ATP generation from electron transfer in the inner membrane.

Although they cannot maintain a stable body temperature, most ectothermic animals (e.g. reptiles) display a behavioural thermoregulation by adjusting organ and cellular metabolism to maintain their

temperature within a relatively narrow range, despite temporal and spatial temperature fluctuations in their habitat [31]. Like in endotherms, their internal heat generation will result essentially from energy transduction in their mitochondria. An impressive testimonial is the selective warming by up to 10-15°C above ambient of the eyes and brain of oceanic predators like swordfishes, which results from specialized heater muscles extremely rich in mitochondria [32,33]. Most invertebrates, plants, fungi and protists have basal metabolic rates that are similar to those of all organisms [11], but they are considered *bona fide* ectotherms because they are unable to control their body temperature. However, in some plants from several families like Araceae (arum lilies) or Cycadacaes (cycads), the flowers are able at specific stages of development to produce unusually large amounts of heat, transiently raising the temperature of their thermogenic tissues up to 35°C above ambient [34]. In the sacred lotus (*Nelumbo nucifera*) and in skunk cabbage (*Symplocarpus sp.*) the flowers display a remarkable physiological thermoregulation since they can maintain for several days a stable temperature in spite of large environmental variations. Flower thermogenesis is only found in ancient plant species, facilitating their reproduction by attracting and providing benefits to insects, in particular beetles, which ensure pollen dispersal and thus fertilization [34]. Depending on the species, heating causes the volatilization of scents (often nauseating, mimicking decaying flesh) that are synthesised by the flower and which strongly attract the pollinators, or it can contribute to offering a shelter to insects during cold nights, improving their energy budget [35]. The fact that respiration of the heating tissues of these flowers was largely resistant to cyanide, which normally blocks mitochondrial respiration by inhibiting complex IV (cytochrome oxidase or COX), led to the discovery of alternative oxidase (AOX), which directly transfers electrons from reduced ubiquinone to oxygen [36] (Figure 1C). AOX was later found to be ubiquitous in plants, playing an important role in the regulation of metabolism and oxidative stress tolerance. AOX genes are generally stress-inducible, and the enzyme regulated by post-translational modifications, therefore, in plants, the AOX pathway activity can be finely adjusted and thus represents a way to uncouple electron transfer from ATP production. In addition to AOX, the ETC in plant mitochondria includes several alternative dehydrogenases (NDx) that transfer electrons from NAD(P)H to ubiquinone without pumping protons (Figure 1C). These alternative dehydrogenases are located on either side of the inner membrane and can thus oxidize NADP(H) of the matrix or of the inter-membrane space [37]. Altogether, the ETC in plant mitochondria appears to be highly branched, with additional pathways like AOX, which bypasses complexes III and IV, and NDx, which bypasses complex I, but also oxidize external NADH (e.g. glycolytic NADH) (Figure 1C). Electron transfer can thus proceed with lower or even no proton pumping, which results in uncoupling energy production from oxidation, and thus heat generation. A detailed expression study of the architecture of ETC in the heating tissues of thermogenic flowers confirmed that electron flow did indeed proceed by using these non-energy conserving pathways [38]. Although plant mitochondria also harbour UCP proteins, they are not believed to play a major role in heat generation in thermogenic flowers, uncoupling resulting rather from the absence of proton pumping.

From this condensed overview of biological heat production, it is clear that mitochondria are the main organelles that generate heat as a by-product of oxidative metabolism in most tissues, and as the primary product in the case of thermogenic tissues. Most organisms are not able to maintain their internal temperature because heat is escaping too fast in the environment, but others have developed various strategies to increase and regulate basal heat production, together with insulation, leading to endothermy. Considering that mitochondria can be considered the universal cellular radiators, a key question is whether, and to what extent, the radiator could be warmer than its surroundings? The development of the first subcellular "thermometers" suggested a slight increase in the temperature within or in the immediate proximity of the organelle [8,9], but interest in these questions surged when mitochondrial temperature was proposed to reach up to 50°C in mammalian cells [6,7].

3. Experimental evidence for mitochondrial warming

Measuring temperature at the micro or even nanoscale is of considerable interest to understand the dynamics of thermal changes in the cell, and their influence on cellular physiology and metabolism. Most approaches to measure temperature rely on the use of fluorescent reporters which properties are modified by temperature, allowing, after calibration, to infer the temperature at their location. A great variety of fluorochromes or flurorophores whith thermosensitive properties have been designed, like inorganic dyes, synthetic polymers, quantum dots, nano-diamonds, but also genetically–encoded fluorescent proteins, which in contrast with the previous sensors, do not need to be loaded within cells. Since we will focus only on mitochondria temperature sensing, the reader is invited to consult a series of recent reviews about intracellular fluorescent thermosensing [39–43].

3.1 Estimation of mitochondrial temperature with thermosensors

To the best of our knowledge, a first application of intracellular thermometry related to mitochondrial heat production was the use of a fluorescent nanogel which was injected into the cytoplasm of COS-7 cells, and allowed to detect an increase of ≈ 1 °C within cells upon uncoupling mitochondrial respiration with FCCP (carbonyl cyanide-4-(trifluoromethoxy)phenylhydrazone), a classical protonophore used to instantly dissipate proton gradient [44]. To increase resolution and accuracy, an improved fluorescent polymeric thermometer (FPT) of smaller size (hydrodynamic diameter < 9 nm) was designed, and after injection in COS-7 cells, time-correlated single photon counting (TCSPS) system-based fluorescence life time imaging (FLIM) was used to image FPT localization, and infer temperature [9]. The advantage of the FLIM-based approach is that the response is independent of the probe concentration, which avoids bias due to heterogeneity of distribution between and within cells. This allowed to analyse temperature heterogeneity in COS-7 or HeLa cells maintained at 30°C, with a resolution of around 0.2-0.6 °C [9]. A systematic higher average temperature difference of +0.96°C between the nucleus and the cytoplasm was observed, which was proposed to result from the high activities related to genome replication and function. Interestingly, the centrosome was also identified

as a frequent hot spot (+ 0.75°C on average), which could reflect intense activities related to cytoskeleton organization [9]. Mitochondria, which were identified by staining with a specific fluorescent marker, were found to localize in the FLIM images at spots corresponding to higher temperature than that of the cytosol, although the images appear to be limited by spatial resolution (Fig 6 and S17 in [9]). FCCP was used to uncouple mitochondria, and thus theoretically enhance heat production of the organelle. Although the average temperature of cells increased by 1°C, it remains difficult to be convinced that the probe allowed visualizing mitochondrial heat production (Fig 6 in [9]). The later development of a new cell-permeable version of the fluorescent polymeric thermometer yielded very similar results [45]. Although the probe was not localized to mitochondria, it nevertheless allowed to image an increase of intracellular temperature following uncoupling with carbonyl cyanide-3-chlorophenylhydrazone (CCCP), as shown in Figure 2A, which was estimated around 1.6 °C. Interestingly, Okabe *et al*. [9] took advantage of the fact that a previous nanogel thermometer has a tendency to moderately aggregate at temperatures over 27°C [44], and therefore examined its distribution with respect to that of several organelles identified with specific fluorescent markers. Indeed, the probe formed more aggregates in regions of COS-7 cells richer in mitochondria than in regions rich in lysosomes, endoplasmic reticulum (ER) or Golgi apparatus (see supplemental figures S11-12 in [9]). Although the images support the hypothesis of mitochondria as the causal factors of aggregation, more data would be needed, in particular on the same cells because mitochondria are often largely represented in ER regions. Besides, probe aggregates found in snapshots should not be forcefully associated to mitochondria clusters because mitochondria are dynamic organelles that travel on cytoskeletal elements, fuse and divide, forming pleomorphic networks or discrete populations within mammalian, yeast and plant cells [46,47]. In another approach, quantum dots showing a heat dependent red shift of emission were introduced into SH-SY5Y neuronal cells, and using two windows for acquisition, a ratiometric value (fluorescence 650-670 nm /fluorescence 630-650 nm) was measured for individual quantum dots, allowing calibration by controlling temperature of the samples [48]. Monitoring of several quantum dots before and after uncoupling mitochondria with 10 µM CCCP revealed increases of temperature of 10 quantum dots with a large variance (up to +6°C) and a mean change of +0.94°C. Clearly, a limitation of these state-of-the-art imaging studies [9,45,48] is the fact that probes were outside of the organelle, which points out to the importance of targeting thermosensors to mitochondria, using fluorescent genetic constructs or specific chemical probes.

A first genetic sensor named tsGFP1 was designed by inserting green fluorescent protein (GFP) sequence within that of TlpA, a thermoresponsive coiled-coil *Salmonella enterica* protein [8]. Temperature increase was shown to causes a rapid and reversible structural transition of tsGFP1 between parallel coiled-coiled dimers and unfolded monomers, modifying the fluorescent properties of the sensor. The excitation spectrum displayed a decrease of the 400 nm peak together with an increase of the 480 nm peak, allowing to calibrate the temperature response of a recombinant tsGFP1 by

measuring the ratio ex400/ex480 of fluorescence emission (510 nm), which yielded a sigmoidal decrease between 20°C and 50°C [8]. This prompted the use of tsGFP1 as a subcellular thermosensor which was targeted to several locations (cytosol, plasma membrane, ER, mitochondria) of HeLa cells by transfection, temperature being estimated in confocal fluorescence images according to the ex400/ex480 of the collected emission (505-525 bandpass). The i*n situ* calibration curves, obtained by varying the temperature of incubation of the culture medium, were similar to that of the purified proteins, allowing to infer the temperature of the targeted compartments [8]. It is worthy of note that while the calibration curve for the cytosolic tsGFP1 was very similar to that of the purified proteins, those for the other compartments were more biphasic, with a steeper slope in the 35-40°C range, which could reflect an influence of the surroundings on the thermosensor properties. When tsGFP1 was expressed in mitochondria of HeLa cells cultured at 37°C, the addition of the 10µM CCCP, which uncouples mitochondrial respiration, caused a sharp and significant decrease of the ex400/ex480 ratio to a new steady-state, which was attributed to mitochondrial thermogenesis, an observation which was supported by the lack of effect of FCCP on tsGFP1 when expressed in the cytosol [8]. The authors also observed a heterogeneity in the response of mitochondria which would reflect differences in thermogenic properties, and interestingly, there was a negative correlation of temperature increase with mitochondrial membrane potential visualized with the JC-1 probe. This strongly suggests that basal thermogenesis was associated with energized mitochondria. When mitochondria were incubated with 10 µM rotenone, an inhibitor of complex I, the ex400/ex480 was slightly higher, reflecting a lower mitochondrial temperature that could results from the lower oxidative phosphorylation activity, and the effect of CCCP was attenuated, which fits with the dampened mitochondrial respiration. The overall data strongly support an increase of mitochondrial temperature in relation to mitochondrial activity (effects of CCCP and rotenone, expected heterogeneity in mitochondrial population), but, surprisingly, the values of temperature were not calculated or discussed. Using the provided *in situ* calibration curve, mitochondrial temperature of control HeLa cells grown at 37°C could be estimated by us at 36-37°C, and thus not warmer than their environment, while uncoupling increased mitochondrial temperature to 42-43°C; in presence of rotenone, mitochondrial temperature would be around 31-34 °C (data from Figures 3 and 4 in [8]). The tsGFP1 sensor was also used to estimate mitochondrial temperature in transfected brown adipocytes from cold-adapted rats. A similar temperature increase in response to CCCP was observed, but interestingly, norepinephrine, which induces thermogenesis by activating lipolysis and UCP1 in BAT tissue was as effective as FCCP, supporting the fact that the thermosensor was indeed able to reflect temperature variations in mammalian cell mitochondria [8]. Overall, this major research led to the possibly first "visualization" of variations of mitochondrial temperature in relation to metabolic activity, but according to the data, at 37°C the temperature of the organelle appeared close to that of its surroundings (cell, medium), although it could indeed increase by 5-6°C upon strong stimulation of oxidative metabolism by uncoupling.

In another strategy, two GFP derivatives with different temperature sensitivities were used to build a ratiometric thermosensor (gTEMP) [49]. The thermosensor relies on the equimolar accumulation of Sirius, a blue emitting protein which fluorescence is strongly affected by temperature, and of mT-Sapphire, a green emitting protein with a much lower temperature sensitivity. Both proteins having overlapping excitation spectra, they can be excited together (around 360 nm) and their ratio of emission (509 nm / 425 nm) was shown to increase by 210 % between 5 and 50°C, with a 2.6 °C %/K temperature sensitivity [49]. To avoid possible fluorescence resonance energy transfer (FRET), the proteins were not expressed as a tandem, but as a fusion construct in which both proteins, each carrying a mitochondrial targeting sequence, were separated by a self-cleavable peptide linker. With this strategy, the proteins were synthesized in the cytosol from the same precursor, and upon cleavage of the linker they were imported separately in the mitochondrial matrix. Upon treatment with 10 µM FCCP, a rapid increase in the 509/425 nm ratio of gTEMP expressed in mitochondria was observed, which corresponded to a 6-9°C increase according to the calibration curve [49]. This rather high value is in line with the 6°C increase triggered by FCCP, that we discussed above in the case of the tsGFP1 thermosensor [8]. However, only a single experiment with a single cell supports the FCCP thermogenic effect visualized with gTEMP, and clearly, more data would be needed. Although the gTEMP approach is very elegant, the expression system remains complex, and it could be important to validate the absence of non-cleaved precursor (that could indeed be imported into mitochondria and interfere through fluorescence resonance energy transfer), and to assess whether the two proteins indeed accumulate to the same extent into mitochondria, which is essential for proper ratiometric analysis. Assuming both proteins have a similar turnover (biosynthesis, import, degradation), since mitochondria form a network and frequently fuse and divide, this could result in a somehow homogenous distribution in the chondriome of these functionally inert proteins.

A recent and promising avenue is the direct use of GFP as a thermosensor, thanks to a small temperature-dependent shift of fluorescence emission that can be used as a ratiometric reporter of temperature [50]. As temperature was increased, recombinant wild-type GFP was shown to display an increase in fluorescence intensity (peak 504 nm at 20°C) that was accompanied by a positive shift of 3 nm between 20 and 60°C. By segmenting the wtGFP peak in two fractions (I_1: 495-504 nm; I_2: 505-600 nm), the author defined a peak fraction parameter $PF = (I_2 - I_1)/I_{total}$ which varied almost linearly as a function of temperature. Because of the limitations of wt-GFP for ectopic expression, the approach was translated to an engineered variant, emGFP, which has been optimized for expression in mammalian cells. The reporter was expressed in mitochondria of HeLa cells, which were incubated at different temperatures for calibrating the PF of emGFP by harvesting fluorescence emission with a confocal microscope equipped for spectral imaging [50]. Although fluorescence intensity decreased with temperature, the thermal sensitivity of the peak shift emGFP was better than that of wtGFP, since a 3 nm shift occurred between 20 and 35°C, and the PF ratiometric measurements could reach 2.2°C

%/K, a value which renders the approach very attractive to monitor mitochondrial temperature using cells transfected with the enhanced GFP. Hela cells expressing em-GFP in mitochondria were thus treated with 10 μM FCCP, which allowed rapid visualization of an increase in mitochondrial temperature (Figure 2B). An average increase of 3-5°C, depending on experiment, was observed when analysing the distribution of em-GFP pixels in several cells (Figure 3 and S10 in [50]). Although the average temperature of mitochondria in all control cells was corresponding to that of the medium (37 °C), the distribution is heterogeneous and reveals hot spots where the temperature can be lower or warmer, possibly reflecting heterogeneity in mitochondrial activities, and hence organelle warming (See Figure 2B). Besides providing evidence in support of mitochondrial warming following uncoupling by FCCP, this work reveals that single GFP variants could be efficiently used as ratiometric thermosensors using spectral imaging. Possibly, other fluorescent proteins could even display stronger shifts, and thus better sensitivity, but in any case, and like in this work, detailed studies will be required to validate their use as thermosensors.

Targeting mitochondria with small molecules endowed with thermosensing properties would provide high resolution without requiring cell transfection or microinjection, and since a variety of fluorescent dyes have been used as mitochondrial markers for decades [51], this led to the design of the first small mitochondrial thermosensors [52,53]. Mito-RTP was constructed by combining a cationic Rhodamine B with a near-infrared emitting dye (CS-NIR), yielding a thermosensor with ratiometric properties since the fluorescence of the rhodamine moiety was decreased by temperature, while that of the CS-NIR was insensitive [53]. Calibration of Mito-RTP was performed by varying the temperature while recording the rhodamine B/ CS-NIR fluorescence emission ratio, which displayed a linear thermal sensitivity of -2.65°C %/K in the 25-43 °C range [53]. Upon incubation with HeLa cells, Mito-RTP was able to penetrate cells and efficiently label mitochondria since the cationic probe is expected to accumulate into the matrix because of the mitochondrial inner membrane potential. Calibration of Mito-RTP *in vivo* was performed by varying the temperature of culture medium, and recording the rhodamine B/ CS NIR fluorescence emission ratio of multiple region of interest (ROIs) yielding a thermal sensitivity (-2.72°C %/K) close to that observed for the probe in solution [53]. In order to demonstrate the capacity of Mito-RTP to sense mitochondrial temperature changes, cells loaded with the probe were treated with 10 μM FCCP. The uncoupler triggered a significant decrease of the rhodamine B/ CS NIR ratio that stabilized after five minutes to a value approximately 10 % lower. The corresponding increase in temperature was not indicated, but the data allows to estimate that FCCP increased temperature by around 3.5-4°C. Although it was concluded that MITO-RTP allowed to visualize FCCP induced mitochondrial thermogenesis, the risk that the cationic probe should not be retained in mitochondria once mitochondrial potential is collapsed by FCCP was not assessed or discussed. Although rhodamines usually equilibrate rapidly in response to membrane potential,

derivatives like Mito-RTP possibly diffuse out of mitochondria slower, as was considered for another rhodamine B derivative used as an ATP sensor [54].

By screening dyes targeting mitochondria for temperature sensitivity, Arai et al (2015) [52] identified a rosamine compound that was named Mito thermo yellow (MTY). The MTY probe was calibrated for temperature response *in vivo* using an intra-cell temperature gradient generated by a NIR laser focusing on aluminium powder at the tip of a microneedle, and measuring the relative fluorescence intensity (F/F_0; F_0 value before heat pulse) as a function of distance [55]. MTY perfectly co-localized with a mitochondrial marker and showed a high temperature sensitivity (2.5-2.8°C %/K) in several types of mammalian cultured cells, but intriguingly the sensitivity was lower (2.0°C %/K) in mouse BAT cells [52]. The authors suggested this could be possibly related to the lower polarization of mitochondria in active BAT cell and stressed the importance of calibrating thermosensors in the cell type of interest. Although MTY appeared as a promising thermosensor, attention was drawn toward the limitations of MTY, in particular because the probe was found to rapidly leak out of mitochondria of HeLa cells upon uncoupling with FCCP (Fig. S6 in [52]). In an earlier report, the same molecule was shown to selectively bind ALDH2 (aldehyde dehydrogenase 2) in murine myoblast and myotube cells [56]. Since ALDH2 is localized in the matrix space, this suggests that MTY fluorescence would report temperature in this compartment. However, the fact that uncoupling causes MTY leakage from mitochondria indicates that most of the probe is not bound, or very weakly, to proteins or other components within the organelle. Another study, that addressed thermogenesis of single-cell brown adipocytes with ERthermAC, a boron-dipyrromethene (BODIPY) derived molecule that target endoplasmic reticulum, allowed to visualize thermal effect triggered by uncoupling adipocytes with 10 µM FCCP [57]. ERthermAC fluorescence decreases with temperature (- 4.76 °C %/K between 35 and 42.8°C), but an absolute calibration was not possible, and the thermal changes thus remain relative. A striking result was that addition of FCCP caused a dramatic drop in the signal of the ER-localized thermosensor, that should represent an average increase in temperature of several °C, that would reflect mitochondrial thermogenenesis caused by uncoupling [57]. Although there is a tight interplay between ER and mitochondria, including the mitochondria-associated membranes (MAMs) that dynamically bridge the organelles [58], such a large and general increase of temperature should in fact concern the whole cell since ER network is widely distributed. The hypothesis is attractive, especially for BAT cells in which ER and mitochondria are in close proximity because of the accumulation of lipid droplets, but it must be stressed that more data, in particular at higher resolution, will be needed to demonstrate that the ER thermosensor can indeed record mitochondrial temperature increase.

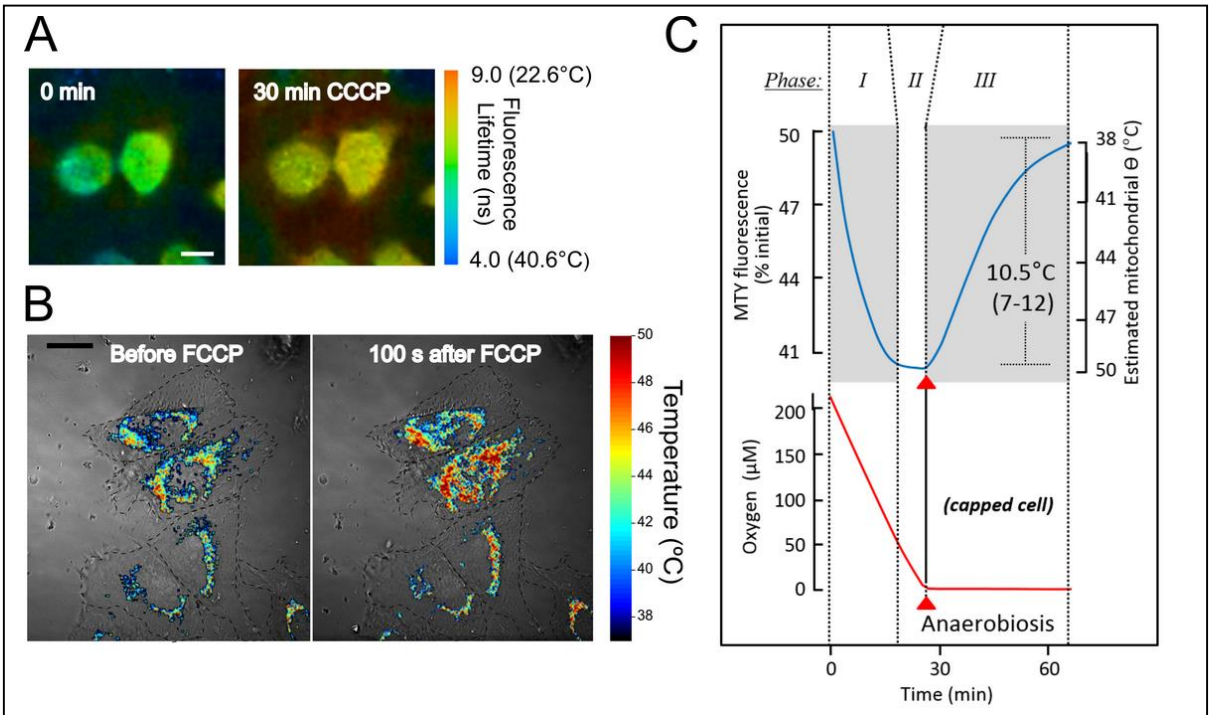

Figure 2. Examples of experiments supporting the hypothesis of a higher temperature in mitochondria. Panel A shows the increase of intracellular temperature which was detected within HeLa cells using the fluorescence life-time of a cell-permeant polymeric sensor, after cells were uncoupled for 30 min with CCCP. The probe was not located in mitochondria but the image and quantitative data (see original paper) suggest a significant increase in cellular temperature. Bar scale = 10 µm. Reproduced from Figure 6 in [45], published under the Creative Commons Attribution 4.0 International Public License (CC BY 4.0; https://creativecommons.org/licenses/by/4.0/). The images in panel B show an increase in mitochondrial temperature within Hela cells which was reported 100 s after addition of the uncoupler FCCP. Here, the temperature within mitochondria was estimated by detecting and measuring the temperature-dependent shift of emGFP-Mito in transfected cells. Quantitative analysis (see original paper) suggests an increase by around 3°C triggered by uncoupling. Bar scale = 20 µm. Reproduced from Figure 3 in [50], published under the Creative Commons Attribution 4.0 International Public License (CC BY 4.0; https://creativecommons.org/licenses/by/4.0/). Panel C illustrates the variations in mitochondrial temperature recorded using suspensions of HEK293 cells loaded with the mitochondrial thermosensor MTY which fluorescence is negatively correlated with temperature. In the experiment MTY fluorescence (blue line) and oxygen concentration (red line) were monitored simultaneously, in a medium thermostated at 38°C. When cells were introduced in the closed cuvette of the spectrophotometer they rapidly consumed the available oxygen due to active mitochondrial respiration (phase I). This active respiration was associated with a decrease of MTY fluorescence that corresponded, according to probe calibration, to an increase in temperature from 38°C to almost 50°C when cells had exhausted all the oxygen and their temperature reaches the maximum (phase II). Then, under anaerobiosis (phase III), mitochondrial respiration was blocked and the organelles progressively cooled down to 38°C. Reproduced from Figure 1 in [6], published under the Creative Commons Attribution 4.0 International Public License (CC BY 4.0; https://creativecommons.org/licenses/by/4.0/).

3.2 A mitochondrial temperature close to 50°C in human cells

As evoked in the introduction, the publication entitled "*Mitochondria are physiologically maintained at close to 50°C*" [6] came into the spotlights because it implied that mitochondria in human cells were maintained at a temperature more than 10°C above that of their tissues because of their inevitable heat production. The authors determined mitochondrial temperature with the MTY thermosensor described above [52], which was used to target the organelle in HEK293 cells and primary fibroblasts. After verifying the mitochondrial localization of MTY, most experiments were performed with HEK293 detached cells loaded with MTY which were studied in a combined system allowing simultaneous spectrofluorimetric and oxygen uptake measurements in controlled temperature conditions [6]. The MTY temperature response (ex 542 nm/ em 562 nm) was first calibrated in solution (between 34-60°C), then *in vivo* by measuring the signal of cells having reached anaerobiosis, and thus not actively respiring, at 38°C, and after stabilization at 41 and 44°C. Because MTY temperature response is almost linear between 30°C and 60°C, and based on this three-step *in vivo* calibration, this allowed to extrapolate mitochondrial temperature from MTY fluorescence signal. Once introduced into the measurement cuvette maintained at 38°C, cells (which have been pre-incubated anaerobically at 38°C) displayed an initial mitochondrial temperature of 38°C that rose steadily to 48.5 °C as oxygen was consumed by respiration (Figure 2C). Once all the oxygen was consumed, the temperature of mitochondria progressively returned to its original value (Figure 2C). When an inhibitor of respiration (0.8 mM KCN, inhibiting cytochrome oxidase) was added during the experiment, the rise in mitochondrial temperature was immediately stopped, and temperature progressively decreased to 38°C. Finally, cells previously depleted of mitochondrial DNA by ethidium bromide treatment, and hence strongly deficient in oxidative phosphorylation (3 % residual cytochrome oxidase capacity) did not display any increase in mitochondrial temperature when transferred to aerobic conditions. This set of experiments [6] strongly supports a link between mitochondrial temperature, as reported by MTY, and mitochondrial activity, and the calibration indeed point out to a mitochondria temperature close to 50°C in cells incubated at 38°C. Unfortunately, experiments with uncouplers (CCCP, FCCP) could not be performed because MTY was shown to rapidly leak out upon addition of the compounds [6,52]. As an alternative, the authors used HEK293 expressing UCP1, which displayed an almost two-fold higher rate of increase in mitochondrial temperature than control cells, leading to a maximum rise of 12 °C, i.e. 50 °C, according the MTY temperature calibration. However, the actual contribution of UCP1 in these experiments remains unknown because it was shown earlier that UCP1-dependent proton leakage in this cell line was strongly dependent on the activation of the protein by fatty acids [59]. Besides, any uncoupling resulting from UCP1 activation should lead to MTY leakage, and we therefore think that more experiments would be needed to link UCP activity to mitochondrial temperature in this cell line. Another series of experiments using respiratory inhibitors strengthened

the link between mitochondrial temperature and oxygen consumption rate, as nicely shown by the effect on both parameters of a dose-response of rotenone, a complex I inhibitor (see Fig 2A in [6]). When ETC inhibitors (KCN, rotenone, antimycin) were used at concentrations that block oxygen consumption, mitochondrial temperature, as deduced from the MTY signal, was observed to regain its initial value corresponding to that of the medium since mitochondrial activity was collapsed. Interestingly, this was also the case with oligomycin, which does not block, but slows down respiration by inhibiting ATPase (see Fig 2B in [6]). In that case, one could expect that state IV respiration should maintain a higher temperature in mitochondria which are still operating electron transfer, albeit at a lower rate. The overall results pointing to such a constitutive high mitochondrial temperature led the authors to determine the optimal temperature of respiratory complex activities measured in crude cell extracts of both HEK293 cells and primary skin fibroblasts (see Fig 4 in [6]. Although these activities are traditionally measured at 37 °C [60], the experiments revealed optimums at around 50°C for several complexes (CIII, CII+CIII, CIV) while that of ATPase was lower (46°C) and that of complex I dropped rapidly above 38°C. Although further investigations would be needed to explain the apparent sensitivity of complex I, these results suggest that human mitochondrial ETC would be indeed adapted to a temperature in the 45-50°C range. It will be nevertheless necessary to measure the optimum temperature of enzyme activities located in "non-thermogenic" cellular compartments (e.g. cytosol, reticulum) to strengthen the concept of higher temperature optima in mammalian mitochondria. On the whole the results of Chrétien *et al.* (2018) rather persuasively suggest a link between mitochondrial activity and organelle temperature. Measurements were performed directly in a spectrophotometer thermostatic cuvette equipped for oxygen measurement, which offers the advantage of precise control of medium temperature which was used for probe calibration with a temperature shift at the end of experiments, when respiration was blocked because of oxygen exhaustion or inhibitors. However, this limits the throughput and replicates, and for most experiments reporting mitochondrial temperature determination, reproducibility is not provided. Another important question concerns the validity of the temperature calibration of the MTY probe since its response is not ratiometric, and fluorescence emission is thus dependent on its concentration in mitochondria, and could also be influenced by proximal environment as cautioned earlier [52]. The spectroflurorometric analyses were carried with whole cell suspensions, and assuming a typical protein content of 150 pg per cell [61], each experiments theoretically represent the response of mitochondrial populations of 2-4 10^7 cells while other studied of mitochondrial thermosensor based on microscopy focus on one or several cells, as discussed before. Intuitively, this huge difference in magnitude would favour the quantitative "large scale" cell study, but conversely, it leads to the loss of any spatial resolution. Whether the MTY signal recorded for whole cell populations always originates from mitochondria cannot be ascertained since the spectrofluorometer harvests fluorescence whatever its localization. The fluorescent micrographs of HEK293 cells treated with FCCP (Fig S3 in [6]) show that the MTY probe that leaked out of mitochondria has invaded the cytosol and would still be

detected although not anymore in mitochondria. In fact, FCCP could have been used as an interesting control to show that, upon uncoupling, the now cytosolic MTY signal should rapidly adjust to medium temperature. Interestingly, the authors also monitored the signal delivered by the endoplasmic reticulum probe ER thermo yellow [55], but the probe appeared not sensitive to strong variations in mitochondrial respiration induced by inhibitors, which supports the idea of mitochondria being warmer than the cytoplasm. This apparently contradicts the sensing of mitochondrial heat production by a ER thermosensor that was reported for BAT cells, but in that case the tight packing of mitochondria and ER between lipid droplets was suggested to favour heat exchange between the organelles [57]. In summary, the cornerstone work of Chretien *et al.* (2018) [6] has added another convincing evidence for mitochondrial heating as a consequence of oxidative metabolism, and possibly uncovered an unexpected temperature of the organelle within mammalian cells. However, deeper investigations are needed to confirm temperature scaling.

A novel small mitochondrial thermosensor (Mito-TEM) that was recently engineered appears very promising because the probe was purposely designed to target and remain in mitochondria independently of membrane potential [62]. Mito-TEM is a cationic rhodamine B derivative displaying high fluorescence thermosensitivity, and that is attracted in mitochondria by membrane potential before binding to proteins thanks to a benzaldehyde reactive group which immobilizes the probe in the organelle. This allowed a precise grayscale calibration of fixed cells, which confirmed the high sensitivity (- 6.50 °C %/K^{-1} between 30 and 40°C) of the probe, and experiments using live cells exposed to different medium temperature or to thermal waves issued from laser irradiation of a heating spot confirmed the responsiveness of Mito-TEM *in vivo*. In another experiment, the authors then treated cells with phorbol 12-myristate 13-acetate (PMA), a drug known to stimulate protein kinase C system, entailing mitochondrial dysfunction, including membrane potential disruption [63]. Image analysis of Mito-TEM signal allowed to demonstrate an increase of mitochondrial temperature by 3°C within a few minutes after treatment, which was attributed to the heat-associated increase in mitochondrial activity caused by the PMA treatment [62]. Although this results appears as another evidence of mitochondrial warming caused by a metabolic change (albeit PMA effect on respiration was not assessed), it would have been more sensible to study the effect of uncouplers since the authors proved that Mito-TEM was retained in mitochondria after treatment with CCCP. Besides the multiple approaches based on chemicals thermosensors delivered in cells, or genetically-encoded fluorescent proteins, another strategy to monitor intra-cellular temperature is the use of miniaturized thermocouples (TC) in the micrometer range [64–66]. Although the technique would benefit from an accurate temperature calibration, it will remain invasive and lack sufficient resolution to monitor temperature at the organelle level. However, such a microscale thermocouple inserted into giant neurons of the sea slug *Aplysia californica* was able to detect intracellular thermal peaks of 7.5±2 °C resulting from uncoupling with the protonophore BAM15 [67]. The fast response rate of the TC

allowed to dissect the temperature transient in a two-component pattern, the first one corresponding to the heat pulse due to dissipation of the mitochondrial membrane potential within one sec, followed by a second-component with slower decay that could reflect modifications in metabolism, and/or delayed thermal emission due to delayed uncoupling or to more distant mitochondria. The fact that thermal increase could not be extended beyond 33 sec suggested that either a higher metabolism could not be sustained longer after uncoupling, or that it was unable to generate an increase in temperature at the probe site [67]. While this approach of direct intra-cellular thermometry does not permit evaluation of mitochondrial warming, it clearly revealed the occurrence of intra-cellular heat waves of mitochondrial origin.

3.3 Mitochondrial temperature in ectotherms

It is also of interest to stress that the experiment we just described above [67] was done with a cold-blooded animal, and, to our knowledge, mitochondrial thermal warming has not been directly addressed yet in other ectotherms. Indeed, if mammalian mitochondria are warmer than their surroundings because of their intrinsic heat production, there is no reason to rule out a similar phenomenon in other organisms. For instance, purified mitochondria isolated from pea seeds were shown earlier to perform OXPHOS with great efficiency at sub-freezing temperature as low as minus 3.5 °C, freezing being prevented because of the osmoticum concentration used in the medium [68]. This is most likely the lowest temperature record for OXPHOS, and in the current context, a contribution of mitochondrial warming to explain the performance of mitochondria at such a low temperature could not be ruled out. Mitochondria self-warming could have maintained a slightly higher temperature of the organelle, hence contributing to maintain its ATP synthesis capacity at very low temperature. Interestingly, efficient oxidative phosphorylation of pea seed mitochondria at sub-freezing temperature could only be achieved using exogenous NADH as a substrate, but not with succinate or complex I substrates. Since this pathway by-passes proton pumping by complex I, it should theoretically lead to the highest amount of energy released as heat during oxidative phosphorylation. It was also reported that pea seeds were able to germinate on ice, which could be related to their capacity to maintain mitochondrial energy transduction at 0°C [68]. Therefore, if mitochondria are indeed warming, even slightly, this could contribute to maintain a better cellular energy status in cells of ectotherms exposed to cold conditions.

3.4 Conclusion about measurements of mitochondrial temperature

To conclude this overview about the measurements of mitochondrial temperature with various techniques that have been performed so far (summarized in Table I), several preliminary conclusions can be drawn. A number of studies using probes located outside of mitochondria have reported increases in temperature of several degrees caused by enhanced mitochondrial activity, generally due to uncoupling which boosts mitochondrial thermogenesis. Several studies using thermosensors located

within mitochondria were able to report an increase in the organelle temperature of several degrees in the same (or similar) conditions, suggesting the mitochondrial radiators could be warmer than their surroundings. Although the study of Chrétien *et al*. [6] revealed a mitochondrial temperature of more than 10°C above that of the culture medium in normal conditions (no uncoupling), such a high difference was not reported or could not be deduced from the other studies. However, heterogeneity in mitochondrial temperature was almost systematically observed, which would be logical because there is large division of labour among the chondriome. Intra-cellular temperature heterogeneity was also observed with non-mitochondrial sensors, which clearly argue against a homogenous instant diffusion of heat at the sub-cellular level. Of course, all the experiments with fluorescent thermosensors are not direct measurements of temperature, and, like any fluorescent probe, they are prone to many artefacts caused by variation in their direct environment (viscosity, pH, ionic strength, quenching…) that can be influenced by mitochondrial function, but also by photo-oxidative reactions (bleaching). We chose not to detail herein the experiments presented in the cited publications to ensure that the responses of the different thermosensors were not affected by variations of such parameters in the physiological range. However, in all cases convincing evidences (e.g. pH and ionic strength responses) were provided using purified probes, validating in principle their applicability *in vivo*.

Table 1. Use of fluorescent thermosensors to study mitochondrial heating and temperature.

Name	Type (R= ratiometric)	Cell type	Localization	Assay	Key results	Reference
1	Nanogel	COS-7	Cytosol	Epifluroescence microscopy	1°C increase upon FCCP addition	[44]
FPT	Polymer (R)	COS-7	Cytosol and nucleus	Fluorescence life time (FLIM) microscopy	Higher temperature around mitochondria, but low resolution. 1-4°C increase upon FCCP addition	[9]
FPT	Nanogel (R)	HeLa, COS-7, mouse NIH/3T3	Cytosol	Fluorescence life time (FLIM) microscopy	Detection of an increase (≈ 1.6°C) in intracellular temperature upon CCCP addition.	[45]
tsGFP1	Genetically-encoded fluorescent protein (R)	HeLa	Mitochondria	Confocal microscopy	Mitochondrial temperature close to that of medium. Increase of 6°C (our estimation) upon FCCP addition. Decrease with rotenone.	[8]
Mito Thermo Yellow (MTY)	Rosamine compound	HeLa, myotubes, embryonic stem cells, mouse BAT	Mitochondria	Confocal microscopy	Temperature responsiveness of MTY was examined in several cellular models, but the effect of uncouplers was not studied.	[52]
Mito-RTP	Rhodamine-CS NIR derivative (R)	HeLa	Mitochondria	Epifluorescence microscopy	Increase in mitochondrial temperature (our estimation 3.5-4°C) upon FCCP stimulation. Organelle temperature heterogeneity was observed.	[53]
QD	Quantum dots (R)	Neuronal SH-SY5Y	Cytosol	Confocal fluorescenc	Detection of up to 6°C increase in temperature upon CCCP treatment. Low throughput.	[48]

				e microscopy		
ATtherm-AC	BODIPY derivative	Adipocytes	Endoplasmic reticulum	Confocal fluorescence microscopy	Detection of an increase in temperature upon FCCP treatment. No calibration.	[57]
gTEMP	Genetically-encoded fluorescent protein (R)	HeLa	Mitochondria	Epifluorescence microscopy	Rapid increase in mitochondrial temperature upon FCCP addition (6°C from our estimation). Organelle temperature heterogeneity was observed.	[49]
Mito Thermo Yellow (MTY)	Rosamine compound	HEK 293, primary skin fibroblasts	Mitochondria	Spectrofluorometry coupled to oxymetry	Mitochondrial temperature increases with respiratory activity, up to 10°C above that of culture medium (38°C). RE temperature remained stable. Optimum temperature of several ETC complexes around 50°C.	[6]
Mito-TEM	Rhodamine derivative	MCF-7	Mitochondria	Confocal fluorescence microscopy	Development of a fixable mitochondrial thermosensor. Increase of 3°C in mitochondrial temperature upon a treatment trieggering mitochondrial dysfunction. Organelle temperature heterogeneity was observed.	[62]
emGFP	Genetically-encoded fluorescent protein (R)	HeLa	Mitochondria	Confocal fluorescence microscopy (spectral imaging)	Average mitochondrial temperature close to that of the medium, but with heterogeneity. Increase of 3-5°C in mitochondrial temperature upon FCCP treatment. Organelle temperature heterogeneity was observed.	[50]

4. The thermal physics point of view

Heat is associated with the microscopic degrees of freedom in materials. Taking the perfect monoatomic gas as an example, the latter reduce to the translational degrees of freedom. In more complex materials the degrees of freedom are associated with the translation of molecules, their rotations, the elastic vibrations of bonds which are very complex to evaluate in general cases. Heat is the kinetic and potential energy that is distributed into these degrees of freedom. If some dissipative processes, such as chemical reactions, release energy in certain locations, the energy will be distributed into the degrees of freedom that are accessible at the temperature of the system. The energy will then be transported away, through the volume of the material. If the material is a good heat conductor, many degrees of freedom can be populated and the freed energy generated by the irreversible processes will diffuse away efficiently, and the temperature rise will be small. On the contrary, if the material is a poor heat conductor the temperature may rise significantly. These thermalization and heat transport processes depend on the properties, the scale and the geometry of the material as well as on the temperature field. In this part, we will review the possibility of having a temperature difference at micrometre scales in biological materials by critically considering all the possible heat transfer processes. We base our analysis on heat transfer in glassy materials, complex materials analogous to cellular media, and on works published in response to the controversy generated by the recent results of Chrétien *et al*. (2018) and by the challenge of thermometry at

nanoscales [8]. For examples the reader may consult the following works: Baffou *et al.* [10] discussed the impossibility of a temperature gradient at the subcellular scale larger than few 10 µK; Suzuki *et al.* [69] discussed the possibility of fluctuation and other nanoscale effects; Leitner *et al.* [70] discussed the energy redistribution within biomolecules and the potential role of interfaces; Lervik et al. [71] focused on geometrical effects; Kang [72] proposed a model of mitochondria energy balance and thermogenesis.

In the first paragraph, we will consider natural convection since it appears to be a very effective mode of heat transfer in liquids with a temperature gradient. Next, we will evaluate the possibility of heat transfer by electromagnetic radiations that represents a lower limit in heat transfer. Finally, we will discuss heat conduction in various ways and show that it overwhelms all other processes. The parameters used to perform the calculations are summarized in supplemental Table I.

4.1 Convection

Convection is a very efficient mode of energy transfer on a large scale. The Rayleigh number (*Ra*) is an adimensional number used to evaluate the possibility of natural convection generated by the difference in buoyancy in liquids induced by a temperature difference. It is formulated from the characteristic length of the system L, the temperature difference, ΔT, between the hot object and the surrounding environment, the acceleration of gravity g, the mass per unit volume ρ, the thermal diffusivity D, the viscosity η and the coefficient of thermal expansion α as:

$$Ra = \frac{\alpha g \Delta T L^3}{\rho \eta D} \quad \text{(Eq. 1)}$$

In the case of mitochondria, the factor L^3 is the most relevant because it reaches 10^{-18} m^3 for a spherical cell of 1 µm in radius while the viscosity cannot be smaller than the viscosity of water 10^{-3} Pa.s; the thermal diffusivity of the cytosol can be estimated from macroscopic measurement on tissues [73] to be higher than 10^{-8} $m^2.s^{-1}$, a conservative value that leads to an overestimation of *Ra*. Similarly, the coefficient of thermal expansion of the cytosol is estimated to be smaller than values around 10^{-3} K^{-1} based on measurements on bacterial cells [74]. A gross calculation of *Ra* yields a value smaller than 10^{-5}. For thermal transfer to occur through convection processes it is generally accepted that Ra> 1800 [75]. Other calculation performed on gold nanodisks 0.5 µm in diameter confirmed that convection currents are not large enough to contribute to heat transfer [76]. Another work has considered spherical geometries that are more appropriate to investigate the possibility of convection current at the subcellular level [77]. Assuming a temperature difference of 10°C between a spherical nucleus and the plasma membrane in a spherical cell, it was shown that convection current can be slightly larger to diffusion current and thus that advection is relevant to heat transport. Transposing this analysis to a spherical mitochondrion imposes a heat dissipation of several µW within the volume of the mitochondria in order to maintain such temperature difference. In summary, if natural

convection occurs it will enhance the heat transfer and thus reduce any temperature difference at the cellular or subcellular level. Thus, it is safe to neglect heat exchange through convection. We are left with radiative or conductive processes.

4.2 Radiation

Electromagnetic radiations are generated by random transitions between the electronic quantum states of molecules and atoms on a surface. The power radiated by the unit surface of the system is expressed according to the Stefan-Boltzmann law as: $P = \varepsilon\sigma T^4$ (Eq. 2), where σ is the Stefan-Boltzmann constant and the emissivity ε is a parameter that is material dependent, which needs to be measured. For water, it is very close to the ideal black body value ε = 1.

In a stationary state, the balance of incoming and outcoming heat fluxes P of a sphere of surface S and emissivity ε_t, and with a small temperature difference ΔT with the surrounding environment can be linearized as :

$$P = 4\varepsilon_t \sigma S T^3 \Delta T \qquad \text{(Eq. 3)}$$

We use this equation to evaluate the temperature of a spherical mitochondrion exchanging power exclusively by radiations. The most disputable parameter in the above equation is the value of the emissivity. It is difficult to measure quantitatively since it depends on wavelength and geometrical factors. Measurements on nanostructured biomaterials in the infrared domain give a conservative lower estimate around 0.2 [78]. Thus, for spherical mitochondria that exchange heat solely by radiation the expected temperature rise for a dissipated power of 1 pW cannot be higher than $60 \cdot 10^{-3}$ K. Although this value is more than two orders of magnitude lower than the highest value observed with a thermosensor [6], it is within experimental reach if no other heat transfer process could take place. In addition, the Stefan Boltzmann law holds for objects much larger than the thermal wavelength [79] set by Wien's displacement law (around 10 µm at 300 K), and mitochondria are clearly under that limit. However, works in the near field limit, i.e. when object size or separation are smaller than the thermal wavelength, showed that the heat transfer is enhanced [80,81]. Thus, for a given power dissipated in the mitochondrion the heat transfer in the near field limit is increased and consequently the temperature difference between the mitochondrion and the cytosol should decrease. In conclusion, a conservative estimate of the temperature difference between the mitochondrion and the cytosol, if thermal radiations were the only transfer process, cannot explain temperature elevations higher than 60 mK. We discuss in the next paragraph the remaining process of energy exchange by thermal conduction, and examine its limits.

4.3 Heat diffusion and temperature

In order to calculate the expected heat flow and consequently the temperature rise in mitochondria, we define which model fits the physical situation in terms of media, sizes, heat carriers and length scales.

Firstly, we discuss the Fourier's law and its spatial limitation (Figure 3). This law describes how heat flow evolves through a solid or a liquid when it is subjected to a gradient of temperature. Which heat carriers are involved? What microscopic mechanisms are at play? These were amongst the first questions that arose. In most crystalline solids, collective modes of vibrations store elastic and kinetic energy and thus the heat carriers are closely related to these modes. Since the cytoplasm consists of water and molecules that are continually vibrating, movement of molecules around their equilibrium positions and configurations will contribute to the transmission of energy. These mechanical vibrations can be quantified in crystalline solids where they are associated with propagating acoustic waves. These vibrating modes are described as quantum quasi-particles referred to as phonon. Like any quantum particle, the phonons have a speed *v*, a wavelength λ and carry an energy *h*ν, *h* being Planck's constant and ν the frequency. As a rule of thumb, small wavelength phonons have higher energy than large wavelength phonons. The intermolecular or interatomic distance generally gives the lower wavelength while the larger wavelength is defined by the system's dimension. The probability for a given phonon to be excited is dependent on the temperature and is given by the black body radiation Planck's law; the higher the temperature, the shorter the phonon wavelength will be. The specific wavelength at which a hot source at a temperature T emits a maximum of phonons is called the dominant phonon wavelength λ_{dom} given by the relation:

$$\lambda_{dom} \approx \frac{h v_s}{2.82 k_B T} \qquad \text{(Eq. 4),}$$

where v_s is the speed of sound and k_B the Boltzmann constant. For instance, for a typical glassy material at room temperature the dominant phonon wavelength is of the order of 1 nm [82]. In the cytoplasm, the speed of sound is close to 1500 m.s^{-1} and the dominant wavelength is of the order of 0.1 nm. This define a length scale below which specific quantum effect should be considered.

As for the particles of an ideal gas, phonons or heat carriers will acquire an average energy at the heat source and as hot carriers will transport this energy along the media toward the cold bath. After being emitted at the hot source, the heat carriers are randomly scattered by obstacles (surfaces, protein interface, boundaries, impurities, and other heat carriers). During these diffusion processes, each heat carrier thermalizes by releasing its energy towards relevant thermodynamic bathes like the phonon bath or the electron bath in metals and toward the molecular degrees of freedom in liquids and mitochondrion. The heat carriers mean free path is the average distance between two scattering events. It is one of the most important lengths for characterizing the transport of heat; the second most important length being the wavelength of the carriers. Indeed, the mean free path *l* sets the value of the heat transport coefficient through the thermal conductivity according to the kinetic law:

$\kappa = 1/3\, \rho c_p v l$, where κ is the thermal conductivity, ρ the density, c_p is the specific heat, and *v* the propagation speed of energy carriers [83]. Very specific thermal effects and the potential invalidity of

Fourier's law may arise if the size of the considered system is smaller than one of these two characteristic length scales [84].

Therefore, Fourier's law is valid when solids or liquids are considered over dimensions that are much larger than all the diffusion length scales. This is equivalent to state that thermal transport (characterized by the quantity called thermal conductivity) must be observed on a sufficiently large length scale in order to be independent on the size of the systems that are under study. On the other hand, for objects of small dimensions, in particular when one of them is smaller than the mean free path of the phonons then the dimensions of the object needs to be considered for understanding the thermal transport, since Fourier's law is no longer valid [85]. The crowded and complex environment of the mitochondrion inner space and of the cytoplasm are in favour of frequent scattering events and thus of the validity of the Fourier's law. Because of the disorder and the absence of long range order the heat transport in the mitochondrion, the cytoplasm or in liquids is analogous to the heat transport in disordered solids like glasses. The mean free path of collective vibrations in a liquid solution is comparable to the mean free path of phonons in an amorphous material like glasses (around 1 nm [86]) or to the interatomic distances (about 0.1 nm in water). Thus, breakdown of the Fourier law cannot be envisaged in the mitochondrion and in the cytoplasm. All-atom and coarse-grained numerical simulations [70] showed that, at the lengthscale of biomolecules, such as proteins or lipids, the temperature homogenises at the time scale of ps. Thus, the temperature field is well-defined at these time and length scales. Therefore, we describe the biological medium as a continuum and by analogy with disordered glassy materials we assign it a poor thermal conductivity.

As a conclusion, we model a mitochondrion as a medium that is composed of water and macromolecules, which has a thermal conductivity κ_m. By analogy with liquid or glassy materials that have no long range order and thus are poor thermal conductors, we assume a range of values for κ_m that spans the thermal conductivity of liquids and glassy materials from $0.1 < \kappa_m < 0.6$, $0.1\ \mathrm{WK^{-1}m^{-1}}$ being the thermal conductivity of typical polymer glass [82] while $0.6\ \mathrm{WK^{-1}m^{-1}}$ is the thermal conductivity of pure water at room temperature. This assumption is valid since the minimal mean free path of molecular vibrations in a liquid solution is set by intermolecular distance, a characteristic length smaller than the characteristic sizes of mitochondrion. Thus, breakdown of the Fourier's law cannot be envisaged in mitochondrion.

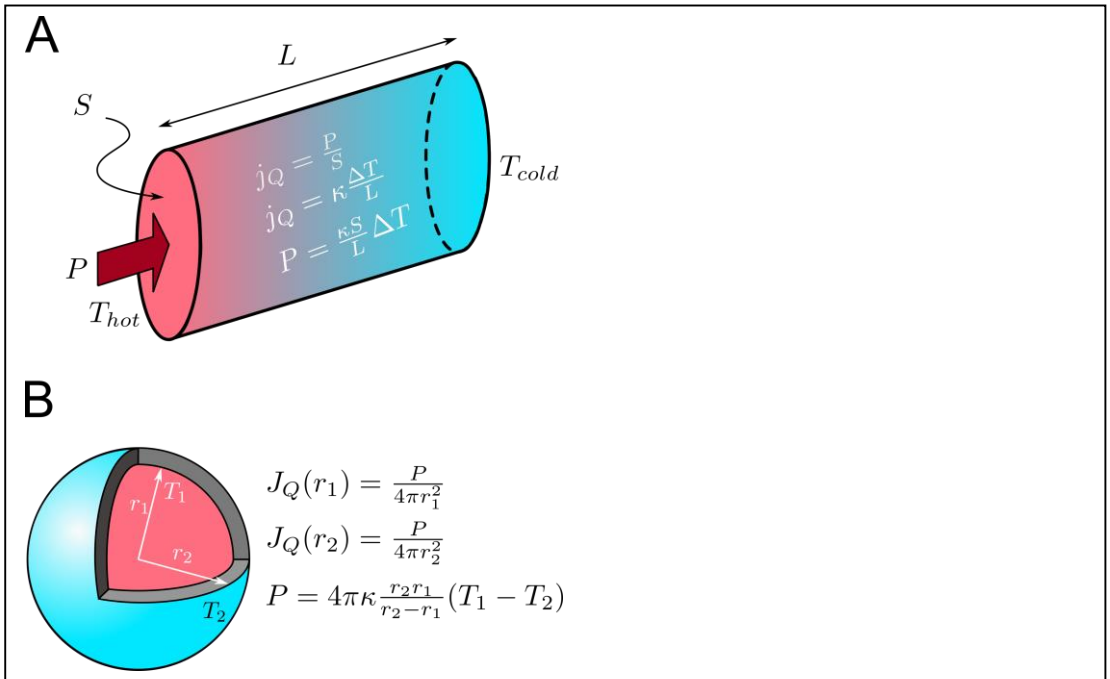

Figure 3. Fourier's law in a simple geometry. Fourier's law links the heat current density $\vec{J}_Q$ to the temperature gradient by defining the thermal conductivity κ a bulk property of materials: $\vec{J}_Q = -\kappa\vec{\nabla}T$. Fourier's law was first devised experimentally by Fourier in 1822 in a macroscopic form $P = K\Delta T$, where P is heat flow expressed in W and K is the thermal conductance in W.K^{-1}. The thermal conductance is related to the thermal conductivity expressed in W. K^{-1}.m^{-1} by geometrical factors. a) In a cylindrical rod of section S in which the heat is transported from one side to another the thermal conductance is $K = \kappa S/L$. b) For a thin spherical shell of thickness $t = r_2 - r_1$ and radius $r = \sqrt{r_1 r_2}$ mimicking the mitochondrion's outer membrane the thermal conductance is expressed as $K_{shell} = \kappa 4\pi r^2/t$. Fourier's law is valid if the transport of heat is diffusive and implies that heat carriers must undergo many scattering events during their erratic journey from the heat source to the cold source. In that limit the heat carriers, phonons in solid materials, or particles and phonons in liquids undergo many scattering events on the length scale of the system. In the opposite limit, the ballistic regime, the thermal conductivity is no longer a bulk property and depends on the geometry of the material.

4.4 Temperature elevation of a mitochondrion assuming Fourier's Law

To calculate the thermal equilibrium of an object with a size of 1 µm, the classical heat transfer equation is entirely appropriate as discussed in the previous paragraph. The temperature field must obey the heat equation that is expressed in a spherical symmetry as:

$$\rho c_p \frac{\partial T}{\partial t} = \kappa \frac{1}{r^2}\frac{\partial}{\partial r} r^2 \frac{\partial T}{\partial r} + s \qquad \text{(Eq. 5)}$$

In short, this equation expresses the conservation of the energy. The left-hand side term represents the local energy storage per unit time. The first term on the right-hand side term is associated with the flow of energy and the second term is the local energy generation per unit time and volume. We cancel out the left-hand side term by considering only stationary solutions $\left(\frac{\partial T}{\partial t} = 0\right)$ to this problem and discuss the validity of this limit at the end of this part. To find the temperature field, we separated the space in regions inside the spherical mitochondrion of radius r_0 where there is an average power source $s = 3P/4\pi r_0^3$ and outside the mitochondrion where there is no power source. As considered earlier, P is the power generated by the processes freeing chemical energy in the mitochondrion, outside the mitochondrion the cytoplasmic thermal conductivity is κ_c and the temperature field is expressed as:

$$T(r) = \frac{P}{4\pi\kappa_c r} + T_0 \qquad \text{(Eq. 6, with } r>r_0\text{)}$$

where we have imposed as boundary conditions that the temperature far from the mitochondrion is T_0 and that the heat flux determined by Fourier's law is $P/4\pi r_0^2$ at the surface of the mitochondrion. Inside the mitochondrion, the power source per unit volume s imposes the following temperature field:

$$T(r) = T_0 + \frac{P}{4\pi r_0}\left(\frac{1}{\kappa_c} + \frac{1}{2\kappa_m}\right) - \frac{P}{8\pi r_0^3}\frac{r^2}{\kappa_m} \qquad \text{(Eq. 7, with } r>r_0\text{)}$$

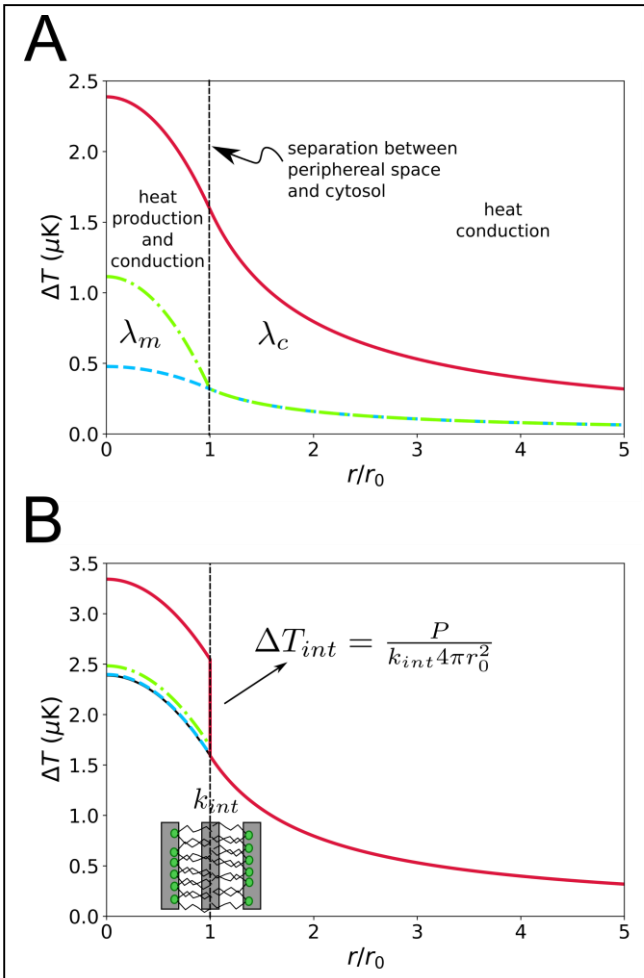

Figure 4. Temperature field as a function of the distance for a spherical mitochondrion dissipating 1pW. The distance is normalised by the mitochondrion's radius r_0. In the inner volume both heat production and heat conduction occur. The dashed vertical lines mark the separation between the inner space of mitochondria ($r < r_0$) and the cytosol ($r > r_0$). In the outer volume, there is no source of heat and only the conduction process takes place. (A) We have considered three different sets of values for the thermal conductivity for the cytoplasm and the mitochondrion matrix, the dashed blue line models the expected temperature field if the thermal conductivities of the medium are close to the thermal conductivity of water: $\kappa_c = \kappa_m =$ 0.5 W.K^{-1}.m^{-1}; dot-dashed and chartreuse green line models a mitochondrial medium with extremely low thermal conductivity: : $\kappa_c =$ 0.5 W.K^{-1}.m^{-1} and $\kappa_m =$ 0.1 W.K^{-1}.m^{-1} , due to the heat production in the mitochondria the temperature rise inside the mitochondria increases; the solid red line models the whole space as an extremely poor thermal conductor: $\kappa_c = \kappa_m =$ 0.1 W.K^{-1}.m^{-1}, nevertheless the temperature elevations stays under measurable limits. (B) The temperature field is plotted considering the Kapitza interface conductance k_{int} placed here arbitrarily between the mitochondrion outer membrane and the cellular media. For the sake of simplicity we pictured three identical interface resistances, dashed blue line $k_{int} = 100\ 10^6$ W.m^{-2}.K^{-1}, dot-dashed and chartreuse green line $k_{int} = 10\ 10^6$ W.m^{-2}.K^{-1} and solid red line $k_{int} = 10^6$ W.m^{-2}.K^{-1} for the same power dissipation within the mitochondrion $P = 10^{-12}$ W and considering extremely poor thermal conductivity in the whole space. The black curve represents the configuration without interface resistances as a reference. The effect of the thermal resistances is seen through a discontinuity in the temperature field at the position of the interface. The lower the thermal conductance the higher the temperature jump. For a thermal conductance as small as 10^6 W.m^{-2}.K^{-1} the temperature rise is maximal but stays below the detection limit.

By solving for the temperature field within the mitochondrial space we extended previous reports [10,72] that considered the temperature field outside mitochondrion. Our aim is to show that no singularity occurs at r=0 as could be suggested by Eq. 6 that is valid only outside mitochondrion.

The temperature field in the whole space, which is represented in Figure 4A, is continuous and in the assumption of very low thermal conductivity in both the cytosol and the mitochondrion's matrix, the expected temperature elevation is maximal at the centre of the mitochondrion and is smaller than 2.5 µK even in the most conservative estimates. Our analysis gives the same conclusion as in Baffou *et al*. [10], namely that a single mitochondrion dissipating a power of the order of the pW cannot generate a measurable temperature elevation anywhere in space. This is assuming that the thermal conductivity remains within reasonable limits and that the relationship between the heat flux and the temperature gradient obeys Fourier's law. In addition, we considered solely the steady state regime which sets up after a typical relaxation time defined by the ratio of the heat capacity divided and the thermal conductance between the mitochondrion and the cytoplasm which is estimated in the next section to be around 10^{-3} WK^{-1}. Thus, for spherical mitochondrion, 1 µm in radius, assuming the specific heat of water and similar density we have a heat capacity of $C \approx 20 \times 10^{-12}$ JK^{-1} which yields a setting time scale for the stationary state of about 20 ns. Kang [72] proposed an initial rate of increase in temperature of about 5 $K.s^{-1}$ basing the reasoning on free energy dissipation due to proton transfer during uncoupling. Such rate of increase of temperature would give a temperature difference of about 10^{-6} K once the stationary state is set, contrasting with results that observed temperature increases of several Kelvin for several minutes [72,87].

Until now, we have modelled mitochondria as homogeneous spheres, albeit with a low thermal conductivity, in contact with an external media also described as homogeneous and with a reduced thermal conductivity with respect to pure water. The complexity of the media has been considered by taking conservative values of the thermal conductivity. However, membranes play crucial roles in biology and particularly in mitochondria by compartmenting space. Along with other phenomena due to interfaces at the molecular scale, we discuss their influence on thermal transport in the next section.

4.5 Emergent and nanoscale effects

In mitochondria, the inner membrane is extensively folded (forming the so-called cristae), and since the membrane is the main site of energy transduction through OXPHOS, the formation of cristae expands the capacity for ATP production by the organelle that remains delimited by the outer membrane (see Fig. 1). Thus, it appears relevant to discuss the effect of interfaces on heat transfer. This includes the contribution of the membrane itself and thermal boundary resistances existing at any interface between two different materials like, for instance, between the membrane (biomaterial) and the cytosol. It is challenging to measure the intrinsic thermal conductivity in biological membranes since the exposed interfaces could contribute significantly to the global thermal conductance of the

system. Non-equilibrium molecular dynamics simulations have been performed on di-palmitoyl-phosphatidylcholine (DPPC) bilayer [88]. The facts that DPPC bilayers are well known to undergo thermodynamic phase transitions as a function of the temperature and that the thermal conductivity of each phase are different, is an additional challenge in these simulations. For temperatures below to 47°C, in the liquid-crystal phase, the thermal conductivity is evaluated to be around $\kappa_{DPPC} \sim 0.5$ W.K^{-1}.m^{-1}. Assuming that Fourier's law holds the thermal conductance of a thin spherical shell of radius r_0 and of thickness t, the equation is expressed as:

$$K = \kappa_{DPPC} \frac{4\pi r_0^2}{t} \qquad \text{(Eq. 8)}$$

Considering that the outer membrane of a mitochondrion is about 6 nm thick and has the same thermal conductivity of DPPC, the total thermal conductance of the outer membrane of the spherical mitochondrion is about K=3.10^{-3} W.K^{-1}. The resulting temperature jump across the interface is of the order of 10^{-9} K which is completely negligible with respect to what has been estimated above. Even if thousands of membrane interfaces were considered it would only give a temperature jump of 10^{-6} K which is not changing our result significantly. Thus, membranes are thermally transparent. We focus in the next paragraph on the interface resistance, which have a larger and subtler contribution in the thermal conduction.

Indeed, there are many models to describe the transfer of phonons at an interface between two media. In the regular Acoustic Mismatch Model [89], developed in the context of ideal and defect free crystalline media in contact at low temperatures, the thermal interface resistance, commonly called the Kapitza resistance, models the capacity of a vibration/phonon wave impinging from medium A to medium B to find available modes of propagations in medium B and to be transmitted. In the other limit, the Diffusive Mismatch Model treats all interfaces as infinitely diffusive. These models yield thermal conductance (more convenient to manipulate than thermal resistance in this case) that are relatively high and of the order of 1 GW.m^{-1}.K^{-1}. However, experimental results can be as low as 100 MW.m^{-1}.K^{-1} down to 1 MW.m^{-1}.K^{-1} for the smallest value ever calculated or measured [90]. Recent studies considering the interface between molecules and water estimated interface thermal conductance to be of the same magnitude, ranging from 10 to 100 MW.m^{-1}.K^{-1} [69,70,91]. The inclusion of a thermal resistance generates a discontinuous temperature jump in the temperature field at interfaces that is evaluated by the following expression:

$$\Delta T_{int} = \frac{1}{k_{int} 4\pi r_0^2} P \qquad \text{(Eq. 9)}$$

The interfaces to be considered are between the intermembrane space and the outer membrane, between the outer membrane and the cytosol and the interface between the two phospholipids, which appear to have the largest contribution in molecular dynamics simulations. By taking the lowest

interface conductance known so far, i.e. ≈ 1 $MW.m^{-1}.K^{-1}$, the temperature jump at the interface pictured in Figure 4B is of the order of 1µK, showing that the thermal interface cannot generate a significant temperature increase by itself. These numbers agree very favourably with the calculations of Baffou *et al*. (2014). The temperature increases obtained using the classical Fourier's law are very low, and consequently, do not give account for what has been recently measured, as already described above. Now, it is necessary to consider the potential effect due to objects of very small sizes, which will be discussed below.

The article by Kiyonaka *et al.* [92] questioned the potential existence of "emergent behaviours" for heat propagation at a very small length scale. As mentioned earlier in this paper, the potential violation of the Fourier's law may appear only if the dimension of the system in which thermal transport has to be calculated becomes smaller than the mean free path of heat carriers. To give an example, a silicon nanowire with a diameter smaller than 100 nm will be in the reduced dimension limit, since the phonon mean free path in bulk silicon is bigger than 300 nm. In that case, the Casimir model can describe the thermal transport where scattering occurs on the boundaries of the system. Then the mean free path l_{nano} is given by the smallest dimensions of the system [93]. For a silicon nanowire, the expected reduction of thermal conductivity, which is due to small dimensions, will be given by the simple relation:

$$\kappa_{nano} = \kappa_{bulk} \frac{l_{nano}}{l_{bulk}} \quad \text{(Eq. 10)}$$

where κ_{nano} and κ_{bulk} stand for the thermal conductivity at the nanometer scale and bulk limit as l_{nano} and l_{bulk} refer to the mean free path in the nanowire and in the bulk. We emphasize that Eq. 10 applies only if $l_{nano} << l_{bulk}$. According to the Casimir model, the smallest dimension, then the diameter, gives the new mean free path at the nanometre scale. The above equation is typically "non-Fourier" since the thermal conductivity depends on the actual geometry of the studied sample [84].

In complex mater such as the cytosol or the mitochondria heat transport can be treated as heat transport in disordered materials such as glassy materials since the mean free path is at the nanometer scale, a scale similar to the intermolecular distances. Collective vibrations, molecular or submolecular rotations are the energy conveyors and molecules diffuse in the media (liquids or glass) with a particular length before being scattered by other molecules. Various experiments on glassy materials at room temperature [86] have confirmed a mean free path, of the order of 1 nm. Thus we expect a similar characteristic length in mitochondria and cellular media. Thus, if we consider the length scales in the mitochondria (size of proteins, membrane thickness, density variations), any effect of reduced dimensions on the thermal transport in the cell can be excluded. From our point of view, the diffusion of the heat in the cell is complex, because it is a heterogeneous medium and therefore this must be

considered in advanced thermal models, but it can, in no case, be taken as an argument to justify orders of magnitude of difference.

4.6 Conclusions regarding thermal modelling for mitochondria

We have shown that the dominating process of heat transfer at subcellular scales is heat conduction. Material properties cannot explain the observed temperature elevation in mitochondria. The spherical geometry, although disputable and over simplified, is the most favourable to limit the heat transport since it is the one that has the smallest surface for a given volume. Our analysis thus confirms the results given by Baffou *et al.* (2014). In addition, we have considered the emerging nanoscale effects that could induce a reduction of the effective thermal conductance. The analysis shows that the temperature elevation within the mitochondrial volume indicated no singularity and that it is non-physical to detect an increase of temperature of about ~1 K, as observed in mitochondria for the estimated power dissipated by the numerous chemical reactions occurring in mitochondria.

5. Some routes to resolve the conundrum

We have seen in this review that it is still impossible to solve the conundrum of the microscopic mitochondrial furnace as being significantly warmer than the cytosol, although a bundle of biological experiments supports this view. We have discussed the known laws of thermal transport and confirmed that they cannot account for the measured temperature increase, and are thus left with the possibility that biological experiments were suffering from artefacts. Physicists models cannot explain the observed temperature rise, but models are general and oversimplify the natural phenomena that occur in order to predict general features. Models should be reconsidered if sound experimental evidence confirms the colossal temperature rise in mitochondrion. In this last part we will therefore put forward some suggestions to resolve uncertainties and possibly explore novel avenues at the interface of mitochondrial biology and physics.

From our survey of the work done so far with the recently developed thermosensors, it is obvious that much more data (including appropriate controls), are needed to prove that mitochondria can indeed be significantly higher in temperature (> 1°C) than their immediate surroundings. In particular, it will be essential to simultaneously measure the temperature of mitochondria and of other compartments (e.g. ER, cytosol) to demonstrate a difference. Fluorescence sensors can be highly sensitive to their physical and chemical environment (pH, ions, oxygen, crowding, viscosity, …), which itself can be altered by the metabolic status, and temperature. In this context, great care must be taken to rule out, or at least consider, such events that could alter the interpretation, and the use of ratiometric sensors should be favoured to eliminate probe concentration effects. In order to increase the confidence, it would be preferable to use different mitochondrial thermosensors in the same experimental model. For microscopical observations, higher resolution and image quality are needed, and all results should be

supported by quantitative data. It would also be important to perform thermosensor experiments using isolated mitochondria. This would allow us to detect any temperature change of the naked organelles as a function of its activity, which could be precisely controlled *in vitro* by the addition of various compounds (substrates, ADP, inhibitors, uncouplers). It would also guarantee a homogenous and stable external temperature and could add much credit to the observations of Chrétien *et al*. (2018). Although it is an invasive and low-throughput approach, the development of microscale thermocouple probes with very fast response [67] appears of interest because it could help resolving high but short-lived intracellular temperature increases that could not be detected with fluorescent sensors. Another promising approach relies on nanodiamond thermometers able to detect temperature changes in the mK range, which were successfully used to measure intracellular submicrometric heat gradient generated by laser heating of gold nanoparticles [94]. In many areas of material sciences such as microelectronics, the design and validation of nanoscale thermometers is a major issue which should foster the development of novel approaches with potential use in life sciences [95].

Energy transduction in mitochondria proceeds out of equilibrium and involves molecular flows and charge transfers which have not been considered explicitly in the power generation of the mitochondria although they may contribute to the overall entropy production. For instance, the proposed occurrence of protonic currents within the inner membrane could possibly challenge the classical view of the system [96]. Such mesoscopic analysis, considering all the molecular fluxes and affinities should be done in order to evaluate the entropy production and thus the dissipated power within the mitochondria. Although calorimetric experiments have been performed earlier with isolated mitochondria [97], we feel that the power dissipated by mitochondria should be quantified by isothermal calorimetry in various conditions in order to establish robust and undisputable values of the heat power generated by mitochondria. Although thermodynamics gives the amount of heat that should be released during OXPHOS, and modelling can help to identify which would be the major steps, we have no real clue of the real sites of heat production at the molecular level within the respiratory chain components, which are not equally distributed, forming super-complexes (See Figure 1B). Finally, our coarse knowledge of the complex landscape in which heat is generated requires more data and modelling from the biophysical side. It would be of interest to design experimental systems to study nanoscale heat dynamics based on simplified membrane models incorporating functional enzymes carrying out reactions with large free energy changes.

To conclude, much effort is needed, and would be worthwhile, to establish whether, or not, mitochondria can be significantly warmer than the cytosol. It will either reconcile biology and physics on the grounds of Fourier's law, or possibly open a novel avenue for both fields.

Acknowledgements

We are thankful to Noriko Inada, Jana Nieder and Pierre Rustin for kindly providing high resolution images of their published papers for reproduction.

Funding:
DM acknowledges the support of the regional programme "Objectif Végétal, Research, Education and Innovation in Pays de la Loire", supported by the French Region Pays de la Loire, Angers Loire Métropole and the European Regional Development Fund.

References

[1] A. Clarke, H.O. Pörtner, Temperature, metabolic power and the evolution of endothermy, Biol. Rev. 85 (2010) 703–727. https://doi.org/10.1111/j.1469-185X.2010.00122.x.

[2] K.A. Nagy, Field metabolic rate and body size, J. Exp. Biol. 208 (2005) 1621–1625. https://doi.org/10.1242/jeb.01553.

[3] D.F.S. Rolfe, G.C. Brown, Cellular energy utilization and molecular origin of standard metabolic rate in mammals, Physiol. Rev. 77 (1997) 731–758. https://doi.org/10.1152/physrev.1997.77.3.731.

[4] W.F. Wright, Early evolution of the thermometer and application to clinical medicine, J. Therm. Biol. 56 (2016) 18–30. https://doi.org/10.1016/j.jtherbio.2015.12.003.

[5] N.A.S. Taylor, M.J. Tipton, G.P. Kenny, Considerations for the measurement of core, skin and mean body temperatures, J. Therm. Biol. 46 (2014) 72–101. https://doi.org/10.1016/j.jtherbio.2014.10.006.

[6] D. Chrétien, P. Benit, H.-H. Ha, S. Keipert, R. El-Khoury, Y.-T. Chang, M. Jastroch, H. Jacobs, P. Rustin, M. Rak, Mitochondria are physiologically maintained at close to 50 °C, PLoS Biol. 16 (2018) e2003992. https://doi.org/10.1101/133223.

[7] N. Lane, Hot mitochondria?, PLoS Biol. (2018) 1–6. https://doi.org/10.1371/journal.pbio.2005113.

[8] S. Kiyonaka, T. Kajimoto, R. Sakaguchi, D. Shinmi, M. Omatsu-Kanbe, H. Matsuura, H. Imamura, T. Yoshizaki, I. Hamachi, T. Morii, Y. Mori, Genetically encoded fluorescent thermosensors visualize subcellular thermoregulation in living cells, Nat. Methods. 10 (2013)

1232–1238. https://doi.org/10.1038/nmeth.2690.

[9] K. Okabe, N. Inada, C. Gota, Y. Harada, T. Funatsu, S. Uchiyama, Intracellular temperature mapping with a fluorescent polymeric thermometer and fluorescence lifetime imaging microscopy, Nat. Commun. 3 (2012) 705. https://doi.org/10.1038/ncomms1714.

[10] G. Baffou, H. Rigneault, D. Marguet, L. Jullien, A critique of methods for temperature imaging in single cells, Nat. Methods. 11 (2014) 899–901. https://doi.org/10.1038/nmeth.3073.

[11] A.M. Makarieva, V.G. Gorshkov, B.A. Li, S.L. Chown, P.B. Reich, V.M. Gavrilov, Mean mass-specific metabolic rates are strikingly similar across life's major domains: Evidence for life's metabolic optimum, Proc. Natl. Acad. Sci. U. S. A. 105 (2008) 16994–16999. https://doi.org/10.1073/pnas.0802148105.

[12] W. Langdon-Brown, Lavoisier and the history of medicine, Proc. R. Soc. Med. 37 (1943) 247–262. https://doi.org/10.1136/bmj.2.3474.205.

[13] S. Nath, The thermodynamic efficiency of ATP synthesis in oxidative phosphorylation, Biophys. Chem. 219 (2016) 69–74. https://doi.org/10.1016/j.bpc.2016.10.002.

[14] S.F. Morrison, K. Nakamura, Central mechanisms for thermoregulation, Annu. Rev. Physiol. 81 (2018) 285–308. https://doi.org/10.1146/annurev-physiol-020518-114546.

[15] G. Abreu-Vieira, C. Xiao, O. Gavrilova, M.L. Reitman, Integration of body temperature into the analysis of energy expenditure in the mouse, Mol. Metab. 4 (2015) 461–470. https://doi.org/10.1016/j.molmet.2015.03.001.

[16] M.L. Reitman, Of mice and men – environmental temperature, body temperature, and treatment of obesity, FEBS Lett. 592 (2018) 2098–2107. https://doi.org/10.1002/1873-3468.13070.

[17] P. Siekevitz, Powerhouse of the Cell, Sci. Am. 197 (1957) 131–144. https://doi.org/10.1038/scientificamerican0757-131.

[18] E. Ferrannini, The theoretical bases of indirect calorimetry: A review, Metabolism. 37 (1988) 287–301. https://doi.org/10.1016/0026-0495(88)90110-2.

[19] A.J. Hulbert, P.L. Else, Mechanisms underlying the cost of living in animals, Annu. Rev. Physiol. 62 (2000) 1–17.

[20] P. Mitchell, Coupling of phosphorylation to electron and hydrogen transfer by a chemi-osmotic type of mechanism, Nature. 191 (1961) 144–148. https://doi.org/10.1038/191144a0.

[21] J.P. Mazat, S. Ransac, M. Heiske, A. Devin, M. Rigoulet, Mitochondrial energetic metabolism

- Some general principles, IUBMB Life. 65 (2013) 171–179. https://doi.org/10.1002/iub.1138.

[22] A.S. Divakaruni, M.D. Brand, The regulation and physiology of mitochondrial proton leak, Physiology. 26 (2011) 192–205. https://doi.org/10.1152/physiol.00046.2010.

[23] A.M. Bertholet, E.T. Chouchani, L. Kazak, A. Angelin, A. Fedorenko, J.Z. Long, S. Vidoni, R. Garrity, J. Cho, N. Terada, D.C. Wallace, B.M. Spiegelman, Y. Kirichok, H+ transport is an integral function of the mitochondrial ADP/ATP carrier, Nature. 571 (2019) 515–520. https://doi.org/10.1038/s41586-019-1400-3.

[24] M.D. Brand, Uncoupling to survive? The role of mitochondrial inefficiency in ageing, Exp. Gerontol. 35 (2000) 811–820. https://doi.org/10.1016/S0531-5565(00)00135-2.

[25] P. Ježek, M. Jabůrek, R.K. Porter, Uncoupling mechanism and redox regulation of mitochondrial uncoupling protein 1 (UCP1), Biochim. Biophys. Acta - Bioenerg. 1860 (2019) 259–269. https://doi.org/10.1016/j.bbabio.2018.11.007.

[26] R. Oelkrug, E.T. Polymeropoulos, M. Jastroch, Brown adipose tissue: physiological function and evolutionary significance, J. Comp. Physiol. B Biochem. Syst. Environ. Physiol. 185 (2015) 587–606. https://doi.org/10.1007/s00360-015-0907-7.

[27] J. Nedergaard, T. Bengtsson, B. Cannon, Unexpected evidence for active brown adipose tissue in adult humans, Am. J. Physiol. - Endocrinol. Metab. 293 (2007) 444–452. https://doi.org/10.1152/ajpendo.00691.2006.

[28] F. Bouillaud, M.C. Alves-Guerra, D. Ricquier, UCPs, at the interface between bioenergetics and metabolism, Biochim. Biophys. Acta - Mol. Cell Res. 1863 (2016) 2443–2456. https://doi.org/10.1016/j.bbamcr.2016.04.013.

[29] J. Nowack, S. Giroud, W. Arnold, T. Ruf, Muscle non-shivering thermogenesis and its role in the evolution of endothermy, Front. Physiol. 8 (2017) 1–13. https://doi.org/10.3389/fphys.2017.00889.

[30] E.T. Chouchani, L. Kazak, B.M. Spiegelman, New advances in adaptive thermogenesis: UCP1 and beyond, Cell Metab. 29 (2019) 27–37. https://doi.org/10.1016/j.cmet.2018.11.002.

[31] A.D. Flouris, C. Piantoni, Links between thermoregulation and aging in endotherms and ectotherms, Temperature. 2 (2015) 73–85. https://doi.org/10.4161/23328940.2014.989793.

[32] K.A. Fritsches, R.W. Brill, E.J. Warrant, Warm eyes provide superior vision in swordfishes, Curr. Biol. 15 (2005) 55–58. https://doi.org/10.1016/j.

[33] B.A. Block, Structure of the brain and eye heater tissue in marlins, sailfish, and spearfishes, J. Morphol. 190 (1986) 169–189. https://doi.org/10.1002/jmor.1051900203.

[34] R.S. Seymour, P. Schultze-Motel, Heat-producing flowers, 21 (1997) 125–129.

[35] R.S. Seymour, C.R. White, M. Gibernau, Heat reward for insect pollinators, Nature. 426 (2003) 243–244. https://doi.org/10.1038/426243a.

[36] A.L. Moore, T. Shiba, L. Young, S. Harada, K. Kita, K. Ito, Unraveling the heater: new insights into the structure of the alternative oxidase, Annu. Rev. Plant Biol. 64 (2013) 637–663. https://doi.org/10.1146/annurev-arplant-042811-105432.

[37] A.G. Rasmusson, D.A. Geisler, I.M. Moller, The multiplicity of dehydrogenases in the electron transport chain of plant mitochondria, Mitochondrion. 8 (2008) 47–60. http://www.sciencedirect.com/science/article/pii/S1567724907002504.

[38] Y. Kakizaki, A.L. Moore, K. Ito, Different molecular bases underlie the mitochondrial respiratory activity in the homoeothermic spadices of Symplocarpus renifolius and the transiently thermogenic appendices of Arum maculatum, Biochem. J. 445 (2012) 237–246. https://doi.org/10.1042/BJ20111978.

[39] K. Okabe, R. Sakaguchi, B. Shi, S. Kiyonaka, Intracellular thermometry with fluorescent sensors for thermal biology, Pflügers Arch. Eur. J. Physiol. (2018) 1–15. https://doi.org/10.1007/s00424-018-2113-4.

[40] J. Qiao, X. Mu, L. Qi, Construction of fluorescent polymeric nano-thermometers for intracellular temperature imaging : A review, Biosens. Bioelectron. 85 (2016) 403–413. https://doi.org/10.1016/j.bios.2016.04.070.

[41] R. Sakaguchi, S. Kiyonaka, Y. Mori, Fluorescent sensors reveal subcellular thermal changes, Curr. Opin. Biotechnol. 31 (2015) 57–64. https://doi.org/10.1016/j.copbio.2014.07.013.

[42] C.D.S. Brites, P.P. Lima, N.J.O. Silva, A. Millán, V.S. Amaral, F. Palacio, L.D. Carlos, Thermometry at the nanoscale, Nanoscale. 4 (2012) 4799–4829. https://doi.org/10.1039/c2nr30663h.

[43] M.M. Ogle, A.D. Smith McWilliams, B. Jiang, A.A. Martí, Latest trends in temperature sensing by molecular probes, ChemPhotoChem. (2020) 1–17. https://doi.org/10.1002/cptc.201900255.

[44] C. Gota, K. Okabe, T. Funatsu, Y. Harada, S. Uchiyama, Hydrophilic fluorescent nanogel thermometer for intracellular thermometry, J. Am. Chem. Soc. 131 (2009) 2766–2767. https://doi.org/10.1021/ja807714j.

[45] T. Hayashi, N. Fukuda, S. Uchiyama, N. Inada, A cell-permeable fluorescent polymeric thermometer for intracellular temperature mapping in mammalian cell lines, PLoS One. 10

(2015) 1–18. https://doi.org/10.1371/journal.pone.0117677.

[46] S. Jakobs, High resolution imaging of live mitochondria, Biochim. Biophys. Acta - Mol. Cell Res. 1763 (2006) 561–575. https://doi.org/10.1016/j.bbamcr.2006.04.004.

[47] D.C. Logan, C.J. Leaver, Mitochondria-targeted GFP highlights the heterogeneity of mitochondrial shape, size and movement within living plant cells, J Exp Bot. 51 (2000) 865–871.

[48] R. Tanimoto, T. Hiraiwa, Y. Nakai, Y. Shindo, K. Oka, N. Hiroi, A. Funahashi, Detection of temperature difference in neuronal cells, Sci. Rep. 6 (2016) 22071. https://doi.org/10.1038/srep22071.

[49] M. Nakano, Y. Arai, I. Kotera, K. Okabe, Y. Kamei, T. Nagai, Genetically encoded ratiometric fluorescent thermometer with wide range and rapid response, PLoS One. 12 (2017) e0172344. https://doi.org/10.1371/journal.pone.0172344.

[50] O.A. Savchuk, O.F. Silvestre, R.M.R. Adão, J.B. Nieder, GFP fluorescence peak fraction analysis based nanothermometer for the assessment of exothermal mitochondria activity in live cells, Sci. Rep. 9 (2019) 1–11. https://doi.org/10.1038/s41598-019-44023-7.

[51] C. Cottet-Rousselle, X. Ronot, X. Leverve, J.F. Mayol, Cytometric assessment of mitochondria using fluorescent probes, Cytom. Part A. 79 A (2011) 405–425. https://doi.org/10.1002/cyto.a.21061.

[52] S. Arai, M. Suzuki, S.-J. Park, J.S. Yoo, L. Wang, N.-Y. Kang, H.-H. Ha, Y.-T. Chang, Mitochondria-targeted fluorescent thermometer monitors intracellular temperature gradient, Chem. Commun. 51 (2015) 8044–8047. https://doi.org/10.1039/C5CC01088H.

[53] M. Homma, Y. Takei, A. Murata, T. Inoue, S. Takeoka, A ratiometric fluorescent molecular probe for visualization of mitochondrial temperature in living cells, Chem. Commun. 51 (2015) 6194–6197. https://doi.org/10.1039/C4CC10349A.

[54] D. de la Fuente-Herreruela, V. Gónzalez-Charro, V.G. Almendro-Vedia, M. Morán, M.Á. Martín, M.P. Lillo, P. Natale, I. López-Montero, Rhodamine-based sensor for real-time imaging of mitochondrial ATP in living fibroblasts, Biochim. Biophys. Acta - Bioenerg. 1858 (2017) 999–1006. https://doi.org/10.1016/j.bbabio.2017.09.004.

[55] S. Arai, S. Lee, D. Zhai, M. Suzuki, Y.T. Chang, A molecular fluorescent probe for targeted visualization of temperature at the endoplasmic reticulum, Sci. Rep. 4 (2014) 6701. https://doi.org/10.1038/srep06701.

[56] Y.K. Kim, J.S. Lee, X. Bi, H.H. Ha, S.H. Ng, Y.H. Ahn, J.J. Lee, B.K. Wagner, P.A. Clemons,

Y.T. Chang, The binding of fluorophores to proteins depends on the cellular environment, Angew. Chemie - Int. Ed. 50 (2011) 2761–2763. https://doi.org/10.1002/anie.201007626.

[57] R. Kriszt, S. Arai, H. Itoh, M.H. Lee, A.G. Goralczyk, X.M. Ang, A.M. Cypess, A.P. White, F. Shamsi, R. Xue, J.Y. Lee, S.C. Lee, Y. Hou, T. Kitaguchi, T. Sudhaharan, S. Ishiwata, E.B. Lane, Y.T. Chang, Y.H. Tseng, M. Suzuki, M. Raghunath, Optical visualisation of thermogenesis in stimulated single-cell brown adipocytes, Sci. Rep. 7 (2017) 1–14. https://doi.org/10.1038/s41598-017-00291-9.

[58] A.R. van Vliet, T. Verfaillie, P. Agostinis, New functions of mitochondria associated membranes in cellular signaling, Biochim. Biophys. Acta - Mol. Cell Res. 1843 (2014) 2253–2262. http://www.sciencedirect.com/science/article/pii/S0167488914000937.

[59] M. Jastroch, V. Hirschberg, M. Klingenspor, Functional characterization of UCP1 in mammalian HEK293 cells excludes mitochondrial uncoupling artefacts and reveals no contribution to basal proton leak, Biochim. Biophys. Acta - Bioenerg. 1817 (2012) 1660–1670. https://doi.org/10.1016/j.bbabio.2012.05.014.

[60] M. Spinazzi, A. Casarin, V. Pertegato, L. Salviati, C. Angelini, Assessment of mitochondrial respiratory chain enzymatic activities on tissues and cultured cells, Nat. Protoc. 7 (2012) 1235–1246. https://doi.org/10.1038/nprot.2012.058.

[61] A. Finka, P. Goloubinoff, Proteomic data from human cell cultures refine mechanisms of chaperone-mediated protein homeostasis, Cell Stress Chaperones. 18 (2013) 591–605. https://doi.org/10.1007/s12192-013-0413-3.

[62] Z. Huang, N. Li, X. Zhang, C. Wang, Y. Xiao, Fixable molecular thermometer for real-time visualization and quantification of mitochondrial temperature, Anal. Chem. 90 (2018) 13953–13959. https://doi.org/10.1021/acs.analchem.8b03395.

[63] Y. Wang, G. Biswas, S.K. Prabu, N.G. Avadhani, Modulation of mitochondrial metabolic function by phorbol 12-myristate 13-acetate through increased mitochondrial translocation of protein kinase Cα in C2C12 myocytes, Biochem. Pharmacol. 72 (2006) 881–892. https://doi.org/10.1016/j.bcp.2006.06.032.

[64] C. Wang, R. Xu, W. Tian, X. Jiang, Z. Cui, M. Wang, H. Sun, K. Fang, N. Gu, Determining intracellular temperature at single-cell level by a novel thermocouple method, Cell Res. 21 (2011) 1517–1519. https://doi.org/10.1038/cr.2011.117.

[65] W. Tian, C. Wang, J. Wang, Q. Chen, J. Sun, C. Li, X. Wang, N. Gu, A high precision apparatus for intracellular thermal response at single-cell level, Nanotechnology. 26 (2015). https://doi.org/10.1088/0957-4484/26/35/355501.

[66] S. Herth, M. Giesguth, W. Wedel, G. Reiss, K.J. Dietz, Thermomicrocapillaries as temperature biosensors in single cells, Appl. Phys. Lett. 102 (2013) 1–5. https://doi.org/10.1063/1.4795289.

[67] M.C. Rajagopal, J.W. Brown, D. Gelda, K. V. Valavala, H. Wang, D.A. Llano, R. Gillette, S. Sinha, Transient heat release during induced mitochondrial proton uncoupling, Commun. Biol. 2 (2019) 1–6. https://doi.org/10.1038/s42003-019-0535-y.

[68] I. Stupnikova, A. Benamar, D. Tolleter, J. Grelet, G. Borovskii, A.-J. Dorne, D. Macherel, Pea seed mitochondria are endowed with a remarkable tolerance to extreme physiological temperatures, Plant Physiol. 140 (2006) 326–335. https://doi.org/10.1104/pp.105.073015.

[69] M. Suzuki, T. Plakhotnik, The challenge of intracellular temperature, Biophys. Rev. 12 (2020) 593–600. https://doi.org/10.1007/s12551-020-00683-8.

[70] D.M. Leitner, H.D. Pandey, K.M. Reid, Energy Transport across Interfaces in Biomolecular Systems, J. Phys. Chem. B. 123 (2019) 9507–9524. https://doi.org/10.1021/acs.jpcb.9b07086.

[71] A. Lervik, F. Bresme, S. Kjelstrup, Heat transfer in soft nanoscale interfaces: The influence of interface curvature, Soft Matter. 5 (2009) 2407–2414. https://doi.org/10.1039/b817666c.

[72] J.-S. Kang, Theoretical model and characteristics of mitochondrial thermogenesis, Biophys. Reports. 4 (2018) 63–67. https://doi.org/10.1007/s41048-018-0054-2.

[73] J.W. Valvano, J.R. Cochran, K.R. Diller, Thermal conductivity and diffusivity of biomaterials measured with self-heated thermistors, Int. J. Thermophys. 6 (1985) 301–311.

[74] K. Nakanishi, A. Kogure, T. Fujii, R. Kokawa, K. Deuchi, R. Kuwana, H. Takamatsu, With respect to coefficient of linear thermal expansion, bacterial vegetative cells and spores resemble plastics and metals, respectively, J. Nanobiotechnology. 11 (2013) 1–7. https://doi.org/10.1186/1477-3155-11-33.

[75] R. Krishnamurti, Some further studies on the transition to turbulent convection, J. Fluid Mech. 60 (1973) 285–303. https://doi.org/10.1017/S0022112073000170.

[76] J.S. Donner, G. Baffou, D. McCloskey, R. Quidant, Plasmon-assisted optofluidics, ACS Nano. (2011) 5457–5462.

[77] R. Howard, A. Scheiner, J. Cunningham, R. Gatenby, Cytoplasmic convection currents and intracellular temperature gradients, PLoS Comput. Biol. 15 (2019) 1–17. https://doi.org/10.1371/journal.pcbi.1007372.

[78] A. Krishna, X. Nie, A.D. Warren, J.E. Llorente-Bousquets, A.D. Briscoe, J. Lee, Infrared optical and thermal properties of microstructures in butterfly wings, Proc. Natl. Acad. Sci. U. S. A. 117 (2020) 1566–1572. https://doi.org/10.1073/pnas.1906356117.

[79] G. Baffou, Thermoplasmonics, Cambridge University Press, 2017. https://doi.org/10.1017/9781108289801.

[80] E. Rousseau, A. Siria, G. Jourdan, S. Volz, F. Comin, J. Chevrier, J.J. Greffet, Radiative heat transfer at the nanoscale, Nat. Photonics. 3 (2009) 514–517. https://doi.org/10.1038/nphoton.2009.144.

[81] K. Kim, B. Song, V. Fernández-Hurtado, W. Lee, W. Jeong, L. Cui, D. Thompson, J. Feist, M.T.H. Reid, F.J. García-Vidal, J.C. Cuevas, E. Meyhofer, P. Reddy, Radiative heat transfer in the extreme near field, Nature. 528 (2015) 387–391. https://doi.org/10.1038/nature16070.

[82] R.O. Pohl, X. Liu, E.J. Thompson, Low-temperature thermal conductivity and acoustic attenuation in amorphous solids, Rev. Mod. Phys. 74 (2002) 991–1013. https://doi.org/10.1103/RevModPhys.74.991.

[83] D.G. Cahill, S.K. Watson, R.O. Pohl, Lower limit to the thermal conductivity of disordered crystals, Phys. Rev. B. 46 (1992) 6131–6140. https://doi.org/10.1103/PhysRevB.46.6131.

[84] O. Bourgeois, D. Tainoff, A. Tavakoli, Y. Liu, C. Blanc, M. Boukhari, A. Barski, E. Hadji, Reduction of phonon mean free path: From low-temperature physics to room temperature applications in thermoelectricity, Comptes Rendus Phys. 17 (2016) 1154–1160. https://doi.org/10.1016/j.crhy.2016.08.008.

[85] A. Tavakoli, K. Lulla, T. Crozes, N. Mingo, E. Collin, O. Bourgeois, Heat conduction measurements in ballistic 1D phonon waveguides indicate breakdown of the thermal conductance quantization, Nat. Commun. 9 (2018). https://doi.org/10.1038/s41467-018-06791-0.

[86] H. Ftouni, C. Blanc, D. Tainoff, A.D. Fefferman, M. Defoort, K.J. Lulla, J. Richard, E. Collin, O. Bourgeois, Thermal conductivity of silicon nitride membranes is not sensitive to stress, Phys. Rev. B - Condens. Matter Mater. Phys. 92 (2015) 1–7. https://doi.org/10.1103/PhysRevB.92.125439.

[87] T.-R. Xie, C.-F. Liu, J.-S. Kang, Sympathetic transmitters control thermogenic efficacy of brown adipocytes by modulating mitochondrial complex V, Signal Transduct. Target. Ther. 2 (2017) e17060. https://doi.org/10.1038/sigtrans.2017.60.

[88] S. Youssefian, N. Rahbar, C.R. Lambert, S. Van Dessel, Variation of thermal conductivity of DPPC lipid bilayer membranes around the phase transition temperature, J. R. Soc. Interface. 14 (2017). https://doi.org/10.1098/rsif.2017.0127.

[89] E.T. Swartz, R.O. Pohl, Thermal boundary resistance, Rev. Mod. Phys. 61 (1989) 605–668. https://doi.org/10.1103/RevModPhys.61.605.

[90] H.K. Lyeo, D.G. Cahill, Thermal conductance of interfaces between highly dissimilar materials, Phys. Rev. B - Condens. Matter Mater. Phys. 73 (2006) 1–6. https://doi.org/10.1103/PhysRevB.73.144301.

[91] H.A. Patel, S. Garde, P. Keblinski, Thermal resistance of nanoscopic liquid-liquid interfaces: Dependence on chemistry and molecular architecture, Nano Lett. 5 (2005) 2225–2231. https://doi.org/10.1021/nl051526q.

[92] S. Kiyonaka, R. Sakaguchi, I. Hamachi, T. Morii, T. Yoshizaki, Y. Mori, Validating subcellular thermal changes revealed by fluorescent thermosensors, Nat. Methods. 12 (2015) 801–802. https://doi.org/10.1038/nmeth.3548.

[93] H.B.G. Casimir, Note on the conduction of heat in crystals, Physica. 5 (1938) 495–500. https://doi.org/10.1016/S0031-8914(38)80162-2.

[94] G. Kucsko, P.C. Maurer, N.Y. Yao, M. Kubo, H.J. Noh, P.K. Lo, H. Park, M.D. Lukin, Nanometre-scale thermometry in a living cell, Nature. 500 (2013) 54–58. https://doi.org/10.1038/nature12373.

[95] M. Quintanilla, L.M. Liz-Marzán, Guiding rules for selecting a nanothermometer, Nano Today. 19 (2018) 126–145. https://doi.org/10.1016/j.nantod.2018.02.012.

[96] A.M. Morelli, S. Ravera, D. Calzia, I. Panfoli, An update of the chemiosmotic theory as suggested by possible proton currents inside the coupling membrane, Open Biol. 9 (2019). https://doi.org/10.1098/rsob.180221.

[97] D. Ricquier, J.L. Gaillard, J.M. Turc, Microcalorimetry of isolated mitochondria from brown adipose tissue. Effect of guanosine-di-phosphate, FEBS Lett. 99 (1979) 203–206. https://doi.org/10.1016/0014-5793(79)80279-3.

[98] T. Brandt, A. Mourier, L.S. Tain, L. Partridge, N.G. Larsson, W. Kühlbrandt, Changes of mitochondrial ultrastructure and function during ageing in mice and Drosophila, Elife. 6 (2017) 1–19. https://doi.org/10.7554/eLife.24662.

[99] D.S. Goodsell, Mitochondrion, Biochem. Mol. Biol. Educ. 38 (2010) 134–140. https://doi.org/10.1002/bmb.20406.